

1 **STARCH SYNTHASE 4 is required for normal starch granule initiation in amyloplasts of**
2 **wheat endosperm**

3

4 Erica Hawkins¹, Jiawen Chen¹, Alexander Watson-Lazowski¹, Jennifer Ahn-Jarvis², J. Elaine
5 Barclay¹, Brendan Fahy¹, Matthew Hartley¹, Frederick J. Warren², David Seung¹

6

7 1. John Innes Centre, Norwich Research Park, Norwich, NR4 7UH, UK

8 2. Quadram Institute, Norwich Research Park, Norwich, NR4 7UQ, UK

9

10

11 Author for correspondence:

12 David Seung

13 +44 1603 450 659

14 David.Seung@jic.ac.uk

15 **SUMMARY**

- 16 • Starch granule initiation is poorly understood at the molecular level. The
17 glucosyltransferase, STARCH SYNTHASE 4 (SS4), plays a central role in granule initiation
18 in Arabidopsis leaves, but its function in cereal endosperms is unknown. We investigated
19 the role of SS4 in wheat, which has a distinct spatiotemporal pattern of granule initiation
20 during grain development.
- 21 • We generated TILLING mutants in tetraploid wheat (*Triticum turgidum*) that are
22 defective in both SS4 homoeologs. The morphology of endosperm starch was examined
23 in developing and mature grains.
- 24 • SS4 deficiency led to severe alterations in endosperm starch granule morphology. During
25 early grain development, while the wild type initiated single 'A-type' granules per
26 amyloplast, most amyloplasts in the mutant formed compound granules due to multiple
27 initiations. This phenotype was similar to mutants deficient in B-GRANULE CONTENT 1
28 (BGC1). SS4 deficiency also reduced starch content in leaves and pollen grains.
- 29 • We propose that SS4 and BGC1 are required for the proper control of granule initiation
30 during early grain development that leads to a single A-type granule per amyloplast. The
31 absence of either protein results in a variable number of initiations per amyloplast and
32 compound granule formation.

33

34 **Keywords:** amyloplast, BGC1, endosperm, granule initiation, SS4, starch, starch synthesis,
35 wheat

36 INTRODUCTION

37 Starch is a major storage carbohydrate in leaves and non-photosynthetic organs of many
38 plants. The starch-rich endosperm of cereal grains is an important source of calories in
39 human diets. Starch forms insoluble semi-crystalline granules that are composed of the
40 glucose polymers - amylopectin and amylose. The biosynthesis of these polymers is
41 relatively well understood and conserved among different plants (Smith & Zeeman, 2020).
42 By contrast, we are only beginning to understand the mechanism of starch granule
43 initiation, and there is vast diversity in the number and morphology of granules between
44 different species and organs (Seung & Smith, 2019).

45

46 There are five major classes of active starch synthases - SS1, SS2, SS3, SS4 and GBSS – which
47 are glucosyltransferases that elongate α -1,4-linked glucan chains of starch polymers using
48 ADP-glucose. SS1, SS2 and SS3 are involved in amylopectin synthesis, and mutants of
49 Arabidopsis and cereals defective in these isoforms have altered amylopectin structure
50 (Wang *et al.*, 1993; Morell *et al.*, 2003; Zhang *et al.*, 2005, 2008; Delvallé *et al.*, 2005; Fujita
51 *et al.*, 2006, 2007; Szydlowski *et al.*, 2011). Amylopectin synthesis also requires branching
52 enzymes (BEs) and debranching enzymes (isoamylases - ISAs) (Delatte *et al.*, 2005; Dumez *et al.*,
53 *et al.*, 2006; Sundberg *et al.*, 2013). Granule-Bound Starch Synthase (GBSS) is required for
54 amylose synthesis (Seung, 2020). In Arabidopsis leaves, SS4 is required for both normal
55 granule initiation and morphogenesis, but does not make a major contribution to
56 amylopectin structure (Roldán *et al.*, 2007; Szydlowski *et al.*, 2009; Crumpton-Taylor *et al.*,
57 2012, 2013; Seung *et al.*, 2017; Lu *et al.*, 2018). While chloroplasts of wild-type leaves
58 contain multiple granules, those of the *ss4* mutant typically contain only one or no granule.
59 The granules of *ss4* have distinct spherical morphology, rather than the flattened shape of
60 wild-type starch granules. The *ss4* mutant also accumulates ADP-glucose, suggesting that
61 other SS isoforms cannot effectively utilise this substrate in the absence of SS4 (Crumpton-
62 Taylor *et al.*, 2013; Ragel *et al.*, 2013).

63

64 Arabidopsis SS4 acts at least partially in complex with other proteins that are required for
65 normal granule initiation. These include PROTEIN TARGETING TO STARCH family members,
66 PTST2 and PTST3 (Seung *et al.*, 2017). PTST2 is proposed to play a role in delivering
67 maltooligosaccharide primers to SS4 for further elongation (Seung *et al.*, 2017). SS4

68 interacts with a coiled-coil protein, MRC (also called PII1), but the exact role of this
69 interaction is unknown (Seung *et al.*, 2018; Vandromme *et al.*, 2019).

70

71 The function of SS4 in non-photosynthetic amyloplasts of storage organs and seeds is
72 unknown. Granule initiation patterns in the endosperm of the Triticeae are radically
73 different from those in Arabidopsis leaves: large, flattened A-type granules initiate early
74 during grain development, and small round B-type granules initiate 10-15 days after the A-
75 type granules (Bechtel *et al.*, 1990; Howard *et al.*, 2011; Chia *et al.*, 2020). Nonetheless, the
76 loss of PTST2 orthologs – FLOURY ENDOSPERM 6 (FLO6) in barley and B-GRANULE CONTENT
77 1 (BGC1) in wheat - has major effects on granule initiation in the endosperm (Suh *et al.*,
78 2004; Saito *et al.*, 2017; Chia *et al.*, 2020). This discovery raises the possibility that granule
79 initiation in wheat endosperm is via an SS4-containing complex, similar to that in
80 Arabidopsis leaves. Here we aimed to generate and characterise wheat mutants that are
81 deficient in *TaSS4*, to determine its role in starch synthesis in the endosperm. The mutants
82 had highly abnormal endosperm starch morphology, resulting from the formation of
83 compound starch granules. Interestingly, this phenotype resembled mutants defective in
84 *TaBGC1* (Chia *et al.*, 2020). Our work demonstrates that both *TaSS4* and *TaBGC1* are
85 required for the control of granule initiation in endosperm amyloplasts.

86

87

88 **MATERIALS AND METHODS**

89 ***Bioinformatics analyses***

90 *TaSS4* loci (Fig. 1) were identified using BLAST against the wheat RefSeq 1.1 genome of
91 cultivar Chinese Spring (Appels *et al.*, 2018) on Ensembl plants (Kersey *et al.*, 2018). *TaSS4*
92 sequences from cultivars Cadenza, Claire, Kronos, Paragon and Robigus were obtained from
93 the Grassroots database (Clavijo *et al.*, 2017).

94

95 *TaSS4* and *TaBGC1* transcript levels during tetraploid wheat grain development were
96 extracted from the datasets of Maccaferri *et al.* (2019) and Xiang *et al.* (2019). Raw RNA-Seq
97 reads obtained from the GenBank Sequence Read Archive (SRA) were processed using
98 Trimmomatic (Bolger *et al.*, 2014) to remove adapter sequences. Processed reads were
99 aligned to the *Triticum turgidum* transcriptome (Maccaferri *et al.*, 2019) using the Quasi

100 align mode in Salmon (Patro *et al.*, 2017) outputting normalised expression as transcripts
101 per million (TPM). Transcript levels of *TaSS4* in different organs of hexaploid wheat were
102 retrieved from the wheat expression database (<http://www.wheat-expression.com>)(Borrill
103 *et al.*, 2016).

104

105 ***Plant materials and growth***

106 Mutants in *Triticum turgidum* (cultivar Kronos) were identified using the wheat *in silico*
107 TILLING resource (<http://www.wheat-tilling.com>)(Krasileva *et al.*, 2017): Kronos2166(K2166)
108 for *TaSS4-1A*, Kronos2565(K2565) and Kronos1450(K1450) for *TaSS4-1B*, and
109 Kronos2275(K2275) for *TaBGC1-4B*. *TaBGC1-4A* mutants, Kronos2244(K2244) and
110 Kronos3145(K3145) are from Chia *et al.* (2020). Plants were crossed to combine A- and B-
111 homoeolog mutant alleles. AA BB, aa BB, AA bb and aa bb genotypes were selected in the F₂
112 generation using KASP V4.0 genotyping (LGC) with the primers in Table S1.

113

114 Wheat plants were grown in controlled environment rooms (CER) or glasshouses at 60%
115 relative humidity with 16 h light at 20°C and 8 h dark at 16°C. The CER light intensity was
116 300 $\mu\text{mol photons m}^{-2} \text{s}^{-1}$. Experiments on leaves and developing grains were carried out on
117 CER-grown material, whereas experiments with mature grains were carried out on either
118 CER or glasshouse-grown material. *Nicotiana benthamiana* plants were grown in
119 glasshouses set to provide a minimum of 16 h light at 22°C, and a dark period of 20°C.
120 *Arabidopsis thaliana* plants were grown in CERs at 60% relative humidity, 12 h light
121 ($150 \mu\text{mol photons m}^{-2} \text{s}^{-1}$)/12 h dark cycles and constant temperature of 20°C.

122

123 ***Starch purification, granule morphology and size distribution***

124 Endosperm starch purification: Mature grains were soaked overnight in ddH₂O at 4°C, then
125 homogenised in a mortar and pestle with excess ddH₂O. Developing grains (stored at -80°C
126 post-harvest) were thawed prior to endosperm dissection and immediately homogenised in
127 ddH₂O using a ball mill at 30 Hz for 1 min. The homogenates were filtered (70 μm nylon
128 mesh) then centrifuged, and the pellet was resuspended into 90% (v/v) Percoll, 50 mM Tris-
129 HCl, pH 8 and centrifuged at 2500g, 5 min. The pellet was washed twice in 50 mM Tris-HCl,
130 pH 6.8, 10 mM EDTA, 4% SDS (v/v), 10 mM DTT and resuspended in ddH₂O.

131

132 Granule morphology was observed using a Nova NanoSEM 450 (FEI) scanning electron
133 microscope (SEM). For cross-polarised light microscopy, the granules were imaged with a
134 DM6000 microscope fitted with a DFC 320F camera (Leica). For analysis of granule size
135 distributions, the starch was suspended into Isoton II (Beckman Coulter), and relative
136 volume vs. diameter plots were generated using a Multisizer 4e Coulter counter (Beckman
137 Coulter) with a 70 μm aperture tube. A minimum of 100,000 particles was measured per
138 sample. All measurements were conducted with logarithmic bin spacing but are presented
139 on a linear x-axis for clarity. The mean diameters of A- and B-type granules, and relative
140 volume fraction of B-type granules, were calculated by fitting a mixture of two log-normal
141 distributions in R (script available at https://github.com/JIC-CSB/coulter_counter_fitting).

142

143 ***Starch quantification, composition and amylopectin structure***

144 Grain starch quantification: Flour (milled in a ball mill; 5-10 mg) was dispersed in 20 μL 80%
145 EtOH, and then incubated with 500 μL thermostable α -amylase in 100 mM sodium acetate
146 buffer, pH 5, at 99°C for 7 min. Amyloglucosidase was added and incubated at 50°C for 35
147 min. All enzymes and reagents were from the Total Starch Assay kit (Megazyme, K-TSTA).
148 The sample was centrifuged at 20,000g for 10 min. Glucose was measured in the
149 supernatant using the hexokinase/glucose-6-phosphate dehydrogenase assay (Roche), for
150 calculation of starch content in glucose equivalents. Leaf starch quantification: 10-day-old
151 seedlings were harvested at the base of the lowest leaf and flash frozen in liquid N_2 . The
152 material was homogenised in 0.7 M perchloric acid using a ball mill at 30 Hz. Insoluble
153 material was pelleted by centrifugation, washed three times in 80% ethanol, then
154 resuspended in water. Starch was digested using α -amylase/amyloglucosidase (Roche), and
155 glucose was assayed as for grains.

156

157 Starch chain length distribution: Purified starch was solubilised and enzymatically
158 debranched using methods adapted from Wu *et al.* (2014), and analysed using high
159 performance size exclusion chromatography (HPLC-SEC) as detailed in Tuncel *et al.* (2019).
160 Calibration curves were generated using pullulan standards (PSS-pulkit, Polymer Standard
161 Service) having peak molecular weights ranging from 342 to 708,000 Da and with
162 correlation coefficients of $R^2 = 0.9997 \pm 0.0002$. The calibration curves were used to
163 determine the relationship between elution volume and hydrodynamic radius (V_h) for the

164 linear glucans, as described by Cave *et al.* (2009). The refractive index elution profiles were
165 converted to SEC weight distributions as described by Perez-Moral *et al.* (2018). Amylose
166 content was determined from chain length distributions as described by Vilaplana *et al.*,
167 (2012). Briefly, the cut-off between amylose and amylopectin in the chain length
168 distribution was set at 100 degrees of polymerisation (D.P.), and the peak areas of the
169 amylopectin (chains <100 D.P.) and amylose (chains >100 D.P.) were integrated. Amylose
170 content was estimated as the ratio of the amylopectin and amylose peak areas expressed as
171 a percentage.

172

173 ***Light and transmission electron microscopy of sections***

174 Mature grain sections: After transverse grain bisection with a razor blade, thin 1 μm
175 sections were produced from the cut surface using an Ultracut UC6 microtome (Leica) fitted
176 with a glass knife. Sections were stained with a 1 in 20 dilution of Lugol's iodine solution
177 (Sigma), and mounted in Histomount (National Diagnostics). Light microscopy was carried
178 out on an AxioObserver Z1 microscope with an AxioCam camera (Zeiss); or a DM6000
179 microscope with a DFC 320F camera (Leica).

180

181 Leaf/developing grain sections: Leaf segments were excised from approximately halfway
182 along the length of a flag leaf (for wheat) or a young rosette leaf (for Arabidopsis), and fixed
183 in 2.5% (v/v) glutaraldehyde in 0.05 M sodium cacodylate, pH 7.3 at 4°C. Developing grains
184 (15 days post anthesis - dpa) were cut in half before immersion in fixative. Using an EM TP
185 embedding machine (Leica, Milton Keynes, UK), samples were post-fixed in 1% (w/v) OsO₄ in
186 0.05 M sodium cacodylate for two hours at room temperature, dehydrated in ethanol and
187 infiltrated with LR White resin (London Resin Company). LR White blocks were polymerised
188 at 60°C for 16 h. For light microscopy, the semi-thin sections (0.5 μm) were prepared. Leaf
189 sections were stained with reagents from the Periodic Acid Schiff kit (Abcam, ab150680), by
190 incubating 30 min in the periodic acid solution and 5 min in Schiff's reagent, then staining
191 with 1% (w/v) toluidine blue for 30 sec prior to mounting in Histomount. Sections from
192 developing grains were stained with 1% (w/v) toluidine blue. Light microscopy was carried
193 out as described above. For transmission electron microscopy (TEM), ultrathin sections
194 (~80 nm) were cut with a diamond knife and placed on formvar and carbon-coated copper
195 grids (EM Resolutions). The sections were stained with 2% (w/v) uranyl acetate for 1 h and

196 1% (w/v) lead citrate for 1 min, washed in distilled water and air dried. Sections were
197 viewed on a Talos 200C TEM (FEI) at 200 kV and imaged with a OneView 4K x 4K camera
198 (Gatan).

199

200 **Visualisation and scoring of starch in pollen**

201 Mature anthers were harvested into 80% (v/v) EtOH and stained with a 1 in 20 dilution of
202 Lugol's iodine solution (Sigma) overnight. After destaining in ddH₂O, pollen was observed
203 with light microscopy as described above. The percentage of starchless pollen (no visible
204 iodine stain) was calculated by scoring the first ≈100 pollen grains observed.

205

206 **Cloning and transformation of plant material**

207 *TaSS4-1A*, *TaSS4-1B*, *TaBGC1-4A* and *TaBGC1-4B* coding sequences were codon optimised to
208 ease sequence complexity and synthesised as gBlocks gene fragments (IDT DNA), flanked
209 with attB1 and attB2 Gateway recombination sites. The optimised sequences are provided
210 in Table S2. The fragment was recombined into the pDONR221 vector using BP Clonase II
211 (Thermo-Fisher). The sequences were recombined into pUBC-YFP (Ubiquitin10-driven
212 expression and C-terminal YFP-tag)(Grefen *et al.*, 2010) or pJCV52 (CaMV 35S-driven
213 expression and C-terminal HA-tag)(Karimi *et al.*, 2002).

214

215 For transient expression in *Nicotiana benthamiana*, *Agrobacterium tumefaciens* (strain AGL-
216 1 or GV3101) harbouring the relevant constructs were grown at 28°C for 48 h. Cultures were
217 resuspended in ddH₂O at OD₆₀₀ = 1.0, and infiltrated into the abaxial leaf surface using a
218 syringe. Proteins were extracted 48-72 h after infiltration. The *TaSS4 1B*-YFP:pUBC-YFP
219 construct was transformed into Arabidopsis by floral dipping (Zhang *et al.*, 2006).

220 Transformants were selected in the T₁ generation using the Basta resistance marker. Basta-
221 resistant individuals from the T₂ or T₃ generation (heterozygous or homozygous for the
222 transgene; single or multiple insertions) with *TaSS4* expression confirmed using
223 immunoblots were used for experiments.

224

225 **Production of antibodies and immunoblotting**

226 To produce *TaSS4* and *TaBGC1* antibodies, the coding sequence of the proteins (minus
227 transit peptide) were amplified using primers in Table S1, and *TaSS4-1B*:pDONR221 or

228 *TaBGC1-4B*:pDONR221 as templates. The amplicons were cloned into the pProExHTb vector
229 (Invitrogen) in frame with the N-terminal His₆-tag using the Gibson assembly master mix
230 (New England Biolabs) for *TaSS4-1B*, or BamHI and XhoI sites for *TaBGC1-4B*. Proteins were
231 expressed in *E. coli* strain BL21 as described in Seung *et al.* (2015). Denaturing purification of
232 the protein with urea was carried out using the Ni-NTA Agarose (Qiagen). Immunisation of
233 rabbits was carried out at Eurogentec. Antibodies were enriched from antiserum using
234 protein A-agarose (Sigma-Aldrich). Affinity purification of *TaBGC1*-specific antibodies from
235 the antiserum was performed with a HiTrap NHS-Activated HP column (GE Healthcare),
236 conjugated to *TaBGC1* recombinant protein.

237

238 For immunoblotting: endosperms from developing grains were dissected and homogenised
239 in 40 mM Tris-HCl, pH 6.8, 5 mM MgCl₂, 2% (*w/v*) SDS, protease inhibitor cocktail (Roche).
240 The homogenate was heated at 95°C for 10 min, and insoluble material was removed by
241 centrifugation at 20,000*g* for 10 min. The concentration of proteins was determined using
242 the BCA assay (Thermo Scientific). The following dilutions of primary antibodies were used
243 for immunoblotting: anti-*TaSS4*: 1:200, anti-*TaBGC1*: 1:200, anti-actin (Sigma-Aldrich;
244 A0480): 1:10,000, anti-YFP (Torrey pines; TP401): 1:5,000, or anti-HA (Abcam; ab91110):
245 1:5,000. Bands were detected using the IRDye 800CW-donkey-anti-rabbit or 680RD-donkey-
246 anti-mouse secondary antibodies (1:10,000; Li-Cor) and the Odyssey Classic Imaging system
247 (Li-Cor).

248

249

250 RESULTS

251 ***Mutants lacking both TaSS4 homoeologs produce aberrant endosperm starch***

252 Hexaploid wheat has three homoeologs of *TaSS4* on group 1 chromosomes (Irshad *et al.*,
253 2019). The B- and D-genome homoeologs were reported to have 16 exons and the A-
254 genome homoeolog has 13 exons. We established that in the most recent wheat genome
255 release (RefSeq v1.1 cv. Chinese Spring; Appels *et al.*, (2018)), these homoeologs correspond
256 to *TaSS4-1A* (TraesCS1A02G353300), *TaSS4-1B* (TraesCS1B02G368500) and *TaSS4-1D*
257 (TraesCS1D02G356900)(Fig. 1a). As reported by Irshad *et al.* (2019), *TaSS4-1B* and *TaSS4-1D*
258 loci contained 16 exons (Fig. 1b) but *TaSS4-1A* had a shorter coding sequence generated
259 from 13 exons. Nonetheless, the predicted transcript length of *TaSS4-1A* was the same as

260 that of the other homoeologs because it had a longer 5' UTR. To investigate the discrepancy
261 in gene model between homoeologs, we compared nucleotide and predicted amino acid
262 sequences from the Chinese Spring reference sequence with those of other sequenced
263 hexaploid wheat cultivars (Cadenza, Paragon, Robigus, Claire) and the tetraploid cultivar
264 Kronos on the Grassroots database (Clavijo *et al.*, 2017)(Fig. S1a). For all cultivars except for
265 Chinese Spring, *TaSS4-1A* was predicted to have all 16 coding exons. Chinese Spring had a
266 unique single nucleotide polymorphism (SNP) that results in a premature stop codon in a
267 position occupied by exon 4 in the gene model for the other cultivars (Fig. 1b,S1a). This SNP
268 most likely led to the incorrect prediction of 13 coding exons and a long 5' UTR for *TaSS4-1A*
269 in the Chinese Spring sequence.

270

271 To assess the importance of *TaSS4* in endosperm starch formation, we created mutants of
272 tetraploid wheat that are defective in both homoeologs of *TaSS4*. We used the TILLING
273 collection of exome-capture sequenced, EMS-mutagenized lines of the tetraploid wheat
274 Kronos (Krasileva *et al.*, 2017; <http://www.wheat-tilling.com>) to identify mutants that are
275 likely to have no *TaSS4-1A* or *TaSS4-1B* protein. The predicted amino acid sequences of
276 *TaSS4-1A* and *TaSS4-1B* from Kronos shared 99-100% identity with those from the Chinese
277 Spring reference genome, and the two Kronos homoeologs were 97% identical to each
278 other (Fig. S1a,b). For *TaSS4-1A*, we obtained the Kronos2166(K2166) line, which carries a
279 splice donor site mutation after exon 5 (Fig. 1b). For *TaSS4-1B*, we obtained
280 Kronos2565(K2565) carrying a premature stop codon in place of Trp364, and
281 Kronos1450(K1450) carrying a splice acceptor site mutation before exon 15. The presence of
282 each mutation was confirmed by KASP genotyping, using the primers in Table S1. The K2166
283 line was crossed with K2565 to create the *Tass4-1* lines, or with K1450 to create the *Tass4-2*
284 lines. KASP genotyping was used to identify F₂ individuals homozygous for both A and B
285 mutations (*aa bb*), homozygous for only the *TaSS4-1A* mutation (*aa BB*) or the *TaSS4-1B*
286 mutation (*AA bb*), and 'negative segregant' controls that lacked both mutations (*AA BB*).
287 Except where specified, observations below were on the *Tass4-1* lines.

288

289 To observe *TaSS4* protein levels during grain development and the effect of the *Tass4-1*
290 mutations on *TaSS4* protein abundance, we generated an antiserum against a *TaSS4-1B*
291 recombinant protein, expressed in and purified from *Escherichia coli*. Immunoblots of

292 *TaSS4-1A* and *TaSS4-1B* proteins transiently expressed in *Nicotiana benthamiana* leaves
293 demonstrated that the antiserum recognised both homoeologs (Fig. S2). Protein extracts
294 from endosperms dissected from wild-type developing grains (10, 15 and 20 days post
295 anthesis (dpa)) were immunoblotted with the antiserum. A band that corresponded to the
296 predicted size of the mature polypeptide (98 kDa) was observed at all three timepoints, but
297 was most prominent at the 10 dpa timepoint (Fig. 2a). Several other bands at different
298 molecular weights were detected, but comparison of immunoblots from the wild-type and
299 mutant extracts showed that the 98 kDa band was missing in the latter while other bands
300 were unaffected (Fig. 2b). We conclude that the 98 kDa band represents *TaSS4*, and that the
301 other bands result from non-specific binding.

302
303 Transcript data for whole caryopses (Maccaferri *et al.*, 2019) and dissected endosperm
304 (Xiang *et al.*, 2019) from developing tetraploid wheat grains revealed that *TaSS4* transcript
305 levels were higher at the early stages of grain development (8-11 dpa) than later stages (16-
306 22 dpa)(Fig. S3). These data are consistent with the observed decrease in *TaSS4* protein
307 levels at later stages of grain development (Fig. 2a).

308
309 To assess the impact of the *Tass4-1* mutations on endosperm starch, we purified starch
310 granules from mature grains and observed them using scanning electron microscopy.
311 Granules from control lines (AA BB) and the single homoeolog mutants (*aa* BB and AA *bb*)
312 had flattened A-type granules and round B-type granules typical of wheat starch (Fig. 3a). By
313 contrast, most starch granules from the double mutant (*aa bb*) had irregular, polyhedral
314 morphology. The irregular granules were highly variable in size, but rarely exceeded the size
315 of a typical A-type granule. A-type granules of normal appearance were also present in the
316 double mutant, but we rarely observed normal B-type granules.

317
318 We used cross-polarised light microscopy to examine the origins of the larger polyhedral
319 granules in the *Tass4-1* double mutant endosperm. In the control line and the single
320 homoeolog mutants, there was one 'Maltese cross' per A-type or B-type granule, indicating
321 a single centre of organisation (Fig. 3b). The few normal A-type granules in the double
322 mutant also had single crosses. However, a complex birefringence pattern with faint or

323 multiple crosses were observed in most of the polyhedral granules, indicating multiple
324 initiation points.

325

326 Using a Coulter counter, we examined the granule size distribution in the endosperm
327 starches. As expected, starch from the control line and single mutants showed a bimodal
328 size distribution, with peaks at approx. 20 μm diameter for A-type and 7-8 μm diameter for
329 B-type granules (Fig. 3c). The size and relative proportion (by volume) of A-type and B-type
330 granules were quantified by fitting a mixed log-normal distribution (Table 1; Tanaka *et al.*,
331 2017). There were no significant differences between the control and single mutants. The
332 granule size distribution of the double mutant had no distinct peaks, and neither a mixed
333 nor a single distribution could be fitted reliably to these data.

334

335 The normal granule morphology of control (AA BB) and single mutant (*aa* BB and AA *bb*)
336 lines indicates that the aberrant morphology arises only when both *Tass4* homoeologs are
337 defective (*aa bb*). However, it remained possible that the aberrant morphology arose from a
338 combination of background mutations in the single-mutant parents of the double mutant.
339 To exclude this possibility, we first backcrossed the double mutant to the wild type twice,
340 and re-isolated the double mutant in the BC₂F₂ generation. Aberrant granule morphology
341 was still observed after the backcrosses (Fig. S4). Granule size distributions of backcrossed
342 and non-backcrossed *Tass4-1 aa bb* lines were identical, indicating that this phenotype is
343 unlikely to arise from background mutations. Second, we examined granule morphology in a
344 second set of mutant lines, *Tass4-2*, obtained by crossing K2166 with an independent
345 mutant for *TaSS4-1B*, K1450 (see above, Fig. 1b). The *Tass4-2 aa bb* double mutant had the
346 same aberrant granule morphology as the *Tass4-1* lines (Fig. S4).

347

348 ***TaSS4* mutations do not alter total starch content, composition or amylopectin structure**

349 We investigated whether the aberrant granule morphology in the *Tass4-1 aa bb* line was
350 accompanied by changes in starch content, composition or structure. The starch content of
351 mature grains was not significantly different on a dry weight basis between control, single
352 and double mutant lines (Table 1). To examine amylopectin/amylose structure and
353 abundance, debranched starch was subjected to High Performance Liquid Chromatography-
354 Size Exclusion Chromatography (HPLC-SEC) with refractive index detection (Cave *et al.*,

2009; Tuncel *et al.*, 2019). The chain length distribution of amylopectin and amylose, and the estimated amylose content, were identical in control and mutant starches (Fig. S5, Table 1). Thus, the altered granule morphology in the *Tass4-1* double mutant cannot be attributed to differences in starch content, composition, or polymer structure.

359

360 ***The Tass4 mutant shows defective granule morphology during early grain development***

361 To investigate at which stage of grain development the aberrant granules in the *Tass4-1*
362 double mutant form, we examined granule morphology and size distribution of starch
363 extracted from developing endosperms at three different time points: 8, 14 and 21 dpa. As
364 expected, the wild-type endosperm contained only A-type granules at 8 dpa, with a peak at
365 approx. 15 µm diameter (Fig. 4a,b). B-type granules were present at 14 and 21 dpa, with a
366 peak at approx. 5 µm diameter. Starch from the *Tass4-1* double mutant already contained
367 aberrant, polyhedral granules at 8 dpa, and no distinct A-type and B-type granule peaks
368 were observed in the mutant at any timepoint.

369

370 ***The Tass4 mutant produces compound granules***

371 We examined the spatial arrangement of the polyhedral granules within the endosperm of
372 the *Tass4-1* double mutant, initially in thin sections of mature grains stained with iodine
373 solution. Consistent with the observations made on purified starch, the control and single
374 mutant lines had normal A- and B-type granules. The granules with polyhedral shapes in the
375 double mutant were almost always tessellated within larger structures (Fig. 5).

376

377 Observing sections of developing endosperm at 15 dpa by light microscopy and TEM
378 revealed remarkable heterogeneity among amyloplasts in the mutant (Fig. 6). Whereas the
379 amyloplasts in the wild type contained single A-type granules and some peripheral stroma,
380 most amyloplasts in the mutant contained compound granules, while some contained A-
381 type granules that were indistinguishable from those of the wild type - and in most
382 endosperm cells, both types of amyloplasts were present. The number of individual
383 'granulae' visible within each compound granule section varied, ranging from 4 to >40.
384 Notably, some amyloplasts had formed granules that were tessellated in tubular structures.

385

386 ***Tass4 starch granules resemble those of the Tabgc1 mutant***

387 The elimination of another component of the putative granule initiation complex defined in
388 Arabidopsis, PTST2/FLO6/BGC1, results in strong granule morphology defects in
389 endosperms of barley and hexaploid wheat, including the occurrence of “semi-compound”
390 granules (Suh *et al.*, 2004; Chia *et al.*, 2020). To discover the relationship between the roles
391 of *TaSS4* and *TaBGC1* in wheat endosperm, we compared phenotypes of *Tass4* and *Tabgc1*
392 mutants in the same Kronos background, and tested whether *TaSS4* and *TaBGC1* proteins
393 can interact with each other. For two *Tabgc1 aa bb* double mutants (Fig. 7a) that
394 accumulate no detectable *TaBGC1* protein (Fig. 2c), we established that starch granules had
395 morphologies like those described for *Tabgc1* mutants in hexaploid wheat and barley:
396 mature grains contained A-type granules of normal appearance and small polyhedral
397 granules (Fig. 7b). As in the *Tass4* mutant, these polyhedral granules were already present
398 during early grain development (8 dpa onwards)(Fig. S6). However, normal A-type granules
399 were more frequent in the *Tabgc1* mutant (Fig. 7b) than in the *Tass4* mutant (Fig. 3a).
400 Coulter counter analysis also showed a prominent A-type granule peak in the *Tabgc1*
401 mutant at a similar diameter to that of the wild type (Fig. 7c, d). Such a distinct peak was not
402 observed in the *Tass4-1* mutant (Fig. 3c).

403

404 ***Loss of TaSS4 affects starch synthesis in pollen***

405 The *Tass4* double mutant was indistinguishable from control lines in terms of plant growth
406 (Fig. 8a). Most grains of the mutant appeared normal and the average weight of individual
407 grains was not significantly altered compared to the wild type, although we observed rare
408 examples of smaller, shrivelled grains in the mutant (Fig. 8b, S7). While the double mutant
409 produced comparable numbers of tillers to the control (Fig. 8c), the number of grains per
410 spike was significantly reduced in the mutant (Fig. 8d). This reduction in grain number was
411 most severe in the non-backcrossed *Tass4-1* double mutant but was partly recovered after
412 backcrossing, suggesting that this phenotype was exacerbated by background mutations in
413 non-backcrossed lines (Fig. 8d). Since the fewer grains in the backcrossed mutant suggests
414 defective fertilisation, we examined starch accumulation in pollen grains of the mutant
415 using iodine staining. Less than a third of pollen grains from the double mutant contained
416 starch, contrasting those from control lines where almost all contained starch (Fig. 8e, S8a).
417 Cross-pollination experiments with the backcrossed *Tass4-1* lines demonstrated that using
418 *aa bb* pollen to fertilise AA BB maternal plants resulted in significantly reduced fertilisation

419 rates compared to the reciprocal cross (Fig. S8b). These data suggest that *TaSS4* is important
420 for normal pollen starch synthesis and viability. Interestingly, grains from low-yielding non-
421 backcrossed and high-yielding backcrossed *Tass4-1* lines had identical starch granule
422 morphology (Fig. S3), demonstrating that this phenotype is independent from the fertility
423 phenotype.

424

425 ***Loss of TaSS4 results in fewer starch granules per leaf chloroplast***

426 Since SS4 plays a critical role in granule initiation and morphogenesis in Arabidopsis leaves,
427 we investigated whether these roles are conserved in wheat leaves. Leaves of the *Tass4-1*
428 double mutant accumulated less than half the starch content of the control over the light
429 period (Fig. 9a). Light microscopy to visualise granules in chloroplasts at the end of the day
430 showed similar frequency distributions of granule sections per chloroplast section in the
431 control and single mutant lines: 70 to 80% of chloroplasts contained between 1-8 granule
432 sections and the remainder contained no visible starch granule (Fig. 9b, c). By contrast,
433 almost 80% of chloroplasts in the double mutant contained no visible starch granule.
434 Examination with TEM showed that granules in control leaves had the typical flattened
435 shape of leaf starch, whereas most granules in the double mutant were small and rounded
436 (Fig. 9d).

437

438 These results suggest that as in Arabidopsis, the loss of *TaSS4* in wheat strongly affects the
439 number of granules initiated per chloroplast. We therefore attempted to complement the
440 Arabidopsis *Atss4* mutant by expression of *TaSS4-1B* with a C-terminal YFP tag and under
441 the Arabidopsis Ubiquitin 10 promoter (pUBQ). The *Atss4-1* mutant had pale leaves, but the
442 transformed lines were not pale (Fig. 10a). The transformed lines had multiple granules in
443 most chloroplasts, whereas most chloroplasts of the *Atss4* mutant were either starchless or
444 contained a single large, round granule (Fig. 10b). *TaSS4* can thus partially complement the
445 granule number phenotype of the *Atss4* mutant. Most granules in the transgenic lines were
446 also irregularly shaped, and few were flattened as in the wild-type, or round as in *Atss4* (Fig.
447 10c) - suggesting *TaSS4* can also influence granule morphology when expressed in
448 Arabidopsis leaves.

449

450

451 DISCUSSION

452 ***TaSS4 is necessary for normal granule initiation in the endosperm***

453 In wheat endosperm, granule initiation is spatially and temporally coordinated such that
454 single A-type granules form in amyloplasts during early grain development and B-type
455 granules initiate later and at least partially in stroma-filled tubules (stromules) that emanate
456 from the amyloplast (Parker, 1985; Langeveld *et al.*, 2000). This pattern is distinct from most
457 other grasses (e.g: rice), which form compound granules by initiating multiple granules per
458 amyloplast during early grain development (Matsushima *et al.*, 2013, 2015). Recent work in
459 Arabidopsis leaves has suggested a mechanism of granule initiation in leaf chloroplasts
460 involving at least six proteins – SS4, SS5, PTST2, PTST3, MFP1 and MRC, each of which is
461 individually necessary for normal granule initiation (Seung & Smith, 2019; Abt & Zeeman,
462 2020). Among these initiation proteins, only SS4 is known to have enzymatic activity (Roldán
463 *et al.*, 2007; Szydlowski *et al.*, 2009; Abt *et al.*, 2020). However, the influence of SS4 on the
464 distinct granule initiation patterns observed in cereal amyloplasts was not known. Our study
465 demonstrates that *TaSS4* is required for the control of granule initiation in wheat
466 endosperm. Loss of *TaSS4* in wheat did not affect the content, composition or polymer
467 structure of endosperm starch (Table 1), but resulted in the formation of compound
468 granules in the endosperm in place of most A-type granules (Fig. 3-6). A similar phenotype
469 was observed in mutants fully deficient in *TaBGC1* in tetraploid wheat (Fig. 7), and in
470 hexaploid wheat (Chia *et al.*, 2020), suggesting that the two proteins act in a similar process.
471 However, the *Tass4* phenotype was more severe than the *Tabgc1* phenotype as there were
472 substantially more normal A-type granules in the latter (Fig. 7). These observations parallel
473 those in Arabidopsis leaves, in which granule initiation is more compromised in the *Atss4*
474 mutant than in the *Atptst2* mutant (Seung *et al.*, 2017).

475

476 To our knowledge, our work provides the first demonstration that SS4 plays a major role in
477 granule initiation in amyloplasts of cereal grains. The severe defects in granule initiation in
478 the *Tass4* mutant is in contrast to the minor defects in compound starch granule
479 morphology in the rice *OsSS4b* mutant (Toyosawa *et al.*, 2016). However, rice has two SS4
480 paralogs, and the extent to which the other paralog (*OsSS4a*) can compensate for the loss of
481 *OsSS4b* in the endosperm is unknown. Interestingly, *OsSS4a* knockout mutants created by
482 gene-editing were observed to have severe defects in plant growth (Jung *et al.*, 2018).

483 Examining endosperm starch in these mutants, as well as in a *oss4a oss4b* double mutant,
484 will be informative of the role of SS4 in a species that already produces compound granules.
485

486 **How do *TaSS4* and *TaBGC1* control the number of granule initiations?**

487 The increase in initiations per amyloplast that leads to compound granule formation
488 following loss of SS4 in wheat endosperm contrasts the reductions in granule number per
489 chloroplast observed in both *Arabidopsis* and wheat leaves (Roldán *et al.*, 2007)(Fig. 9).
490 Thus, in wheat endosperm, neither *TaSS4* nor *TaBGC1* is strictly required for the initiation of
491 granules *per se*, but both are required to control the process - such that single A-type
492 granules initiate in amyloplasts during early grain development. It remains to be determined
493 how these proteins exert this control. It is possible that *TaSS4* and *TaBGC1* together form a
494 single granule initiation per amyloplast, from which the other enzymes of starch
495 biosynthesis can build a single A-type granule (Fig. 11). The formation of this single granule
496 initiation may be enough to suppress the formation of more granules – since the activity of
497 other starch biosynthesis enzymes can be directed towards the growing granule. However,
498 in the absence of this single granule initiation, the other enzymes may start elongating any
499 available substrate, such as soluble maltooligosaccharides, leading to an uncontrolled
500 number of granules being initiated. These enzymes may include starch synthases and starch
501 phosphorylase, which can all elongate maltooligosaccharides *in vitro* (Hwang *et al.*, 2010;
502 Brust *et al.*, 2013; Cuesta-Seijo *et al.*, 2016). The heterogeneity in granule number among
503 amyloplasts in the endosperm of *Tass4* and *Tabgc1* mutants may reflect stochasticity in the
504 number of initiations per amyloplast that occur in the absence of SS4 or BGC1. It is also
505 possible that some amyloplasts fail to initiate starch granules, but it is very difficult to
506 distinguish empty amyloplasts from other membranous structures in TEM images of the
507 endosperm.

508

509 It is unknown which features of *TaSS4* allow it to initiate a single granule per amyloplast.
510 Notably, distinct patterns of protein localisation have been observed for *AtSS4* in
511 *Arabidopsis* leaves, and for *OsSS4b* in rice amyloplasts - where it locates to the septum-like
512 structures of compound granules (Toyosawa *et al.*, 2016). We are currently exploring the
513 localisation of *TaSS4* in amyloplasts of developing grains and whether that could explain a
514 single point of A-type granule initiation. Since granule initiation proteins in *Arabidopsis*

515 leaves act via protein-protein interactions, searching for interacting proteins may also
516 provide insight on how *TaSS4* and *TaBGC1* act in wheat endosperm. *AtSS4* is proposed to
517 interact with *AtPTST2* in Arabidopsis leaves (Seung *et al.*, 2017). Although we attempted
518 multiple co-immunoprecipitation and pulldown approaches, we failed to find any evidence
519 that *TaSS4* and *TaBGC1* interact in the endosperm (data not shown). Further work is
520 required to determine if they interact only weakly or transiently. Possible interactions of
521 these proteins with ISOAMYLASE 1 (*ISA1*) should also be investigated since *ISA1* is reported
522 to interact with *PTST2* (*FLO6*) in rice (Peng *et al.*, 2014). Notably, *isa1* mutants of barley
523 contain compound granules that resemble those of the *Tass4* mutants (Burton *et al.*, 2002),
524 providing a strong indication for *ISA1* involvement in granule initiation.

525
526 The specific role of *TaSS4* in B-type granule initiation must also be further explored. Very
527 few normal round B-type granules were observed in mature grains of the *Tass4* mutant (Fig.
528 3). Also, at 15 dpa, we observed many compound granules in a linear arrangement in the
529 mutant, raising the possibility that they formed in stromules that normally enclose B-type
530 granules (Fig. 6). Interestingly, Chia *et al.* (2020) reported that reducing gene dosage of
531 *TaBGC1* in hexaploid wheat can almost eliminate B-type granules while retaining normal A-
532 type granule morphology. By contrast, B-type granule volume was not affected in either of
533 the single homoeolog mutants in *TaSS4*, but it is possible that a further reduction in gene
534 dosage is required to see an effect. However, we noted that while *TaSS4* protein levels are
535 highest during early grain development and decrease at the later developmental stages,
536 *TaBGC1* transcript and protein levels increase and are highest during the period of B-type
537 granule initiation (Fig. 2; Fig. S3). Thus, it is possible that *TaBGC1* has a specific role during B-
538 type granule initiation that is independent of *TaSS4*.

539
540 While other members of the Triticeae (e.g., barley and rye) also have A- and B-type
541 granules, most other grasses produce compound granules in the endosperm (Matsushima *et*
542 *al.*, 2013, 2015). The fact that loss of *SS4* or *BGC1* gives rise to some compound granules in
543 wheat makes it tempting to speculate that differences in the extent and timing of *SS4*
544 and/or *BGC1* expression between species could determine whether a given species
545 possesses compound granules. However, the difference between compound and other
546 patterns of granule initiation is unlikely to be so simple. Compound granules of rice have

547 complex structural features, including membranes and septum-like structures that separate
548 each constituent granula (Yun & Kawagoe, 2010; Kawagoe, 2013; Toyosawa *et al.*, 2016).
549 Thus, the formation of compound granules in rice is likely to involve multiple genes that
550 control starch synthesis and amyloplast morphogenesis.

551

552 ***TaSS4 is required for proper granule initiation in leaves and pollen***

553 In leaves of the Arabidopsis *Atss4* mutant, over 75% of chloroplasts had no visible starch
554 granule, and the majority of remaining chloroplasts contained one large granule (Roldán *et*
555 *al.*, 2007; Seung *et al.*, 2017). Leaves of the *Tass4* mutant had a percentage of starchless
556 chloroplasts that was comparable to the Arabidopsis mutant, but the remaining chloroplasts
557 mostly contained multiple granules (Fig. 9). The reason for this difference between the
558 Arabidopsis and wheat phenotypes is unknown, but could reflect differences in the
559 compensation mechanism following loss of SS4. The few granules present in the Arabidopsis
560 *Atss4* mutant are likely initiated by SS3, since the *Atss3 Atss4* double mutant is almost
561 starchless (Szydlowski *et al.*, 2009; Seung *et al.*, 2016). Further work is required to
562 determine whether SS3 initiates the starch granules in leaves of the *Tass4* mutant.

563

564 The expression of *TaSS4*, which shares 56% amino acid sequence identity with *AtSS4* (BLAST
565 pairwise alignment), could largely restore the initiation of multiple granules per chloroplast
566 when expressed in the Arabidopsis *Atss4* mutant. However, the exact role of *TaSS4* in
567 granule morphogenesis in leaves remains unclear. Starch granules in the *Tass4* mutant were
568 small and round (Fig. 9), but distinct from the large, rounded granules of the *Atss4* mutant
569 (Fig. 10). *TaSS4* expression in the *Atss4* mutant resulted in aberrant granule morphology,
570 which was distinct from both the round granules of *Atss4* and the flattened granules of the
571 wild type. These aberrant granule shapes may result from partial complementation by
572 *TaSS4* that achieves an 'intermediate' morphology between round and flattened, or
573 abnormal function of *TaSS4* in Arabidopsis leaves (e.g., due to missing interaction partners
574 or other regulatory factors).

575

576 Despite a reduction in gene dosage to 50% in our single homoeolog wheat mutants, we did
577 not observe an effect on granule number in leaf chloroplasts. On first glance, this is in
578 contrast to a previous report that hexaploid wheat mutants deficient in only *TaSS4-1D* have

579 reduced numbers of granules per chloroplast (Guo *et al.*, 2017). However, we showed that
580 some hexaploid cultivars, including the reference cultivar Chinese Spring, have a natural
581 polymorphism that leads to a premature stop codon in *TaSS4-1A* (Fig. 1). It is possible that
582 *TaSS4-1B* is the only functional homoeolog in the *TaSS4-1D* mutants of Guo *et al.* (2017)(in
583 cultivar Jing411), and thus may have a functional gene dosage of only 33%.

584

585 *TaSS4* also appears to be required for normal starch synthesis in wheat pollen. Publicly
586 available gene expression data for hexaploid wheat suggests that *TaSS4* is expressed in
587 microspores in addition to leaves, stems, roots and grains (Fig. S3b); and most pollen grains
588 from our *Tass4* mutants were starchless (Fig. 8e, S8). In rice, starch synthesis in pollen
589 appears to be essential for viability, as rice *pgm* mutants lacking pollen starch are sterile
590 (Lee *et al.*, 2016). Consistent with this, the pollen from the *Tass4* mutant had significantly
591 reduced fertilisation success in cross-fertilisation experiments (Fig. S8b), and the mutants
592 produced fewer grains per spike (Fig. 8d, S8c). These grains likely result from the small
593 proportion of mutant pollen that contains starch. Further work should examine the effects
594 on granule number and morphology in these starch-containing pollen grains.

595

596

597 **ACKNOWLEDGEMENTS**

598 This work was funded through a John Innes Foundation (JIF) Chris J. Leaver Fellowship (to
599 D.S), a Biotechnology and Biological Sciences Research Council (BBSRC, UK) Future Leader
600 Fellowship BB/P010814/1 (to D.S.), a JIF Rotation Ph.D. studentship (to J.C.) and BBSRC
601 Institute Strategic Programme grants BBS/E/J/000PR9790 and BBS/E/J/000PR9799 (to the
602 John Innes Centre). FJW and JAJ were funded through Quadram BBSRC Institute Strategic
603 Programme grant Food Innovation and Health BB/R012512/1 and its constituent projects
604 BBS/E/F/000PR10343, BBS/E/F/000PR10345 and BBS/E/F/000PR10346. We gratefully
605 acknowledge: Prof. Alison Smith (JIC) for critical reading of this manuscript and her valuable
606 advice throughout the course of this work, Dr. Kay Trafford (NIAB) for critical reading of this
607 manuscript and helpful discussions on granule initiation in wheat, Prof. Cristobal Uauy (JIC)
608 and Dr. Philippa Borrill (University of Birmingham) for their invaluable advice on wheat
609 research. We also thank Dr. George Savva (Quadram Institute) for advice on statistical
610 analysis, and James McLaughlin and Olivia Mohr (JIC) for technical assistance. We thank the

611 JIC Horticultural Services for providing growth facilities and maintenance of plant material,
612 JIC Bioimaging for providing access to microscopes, and the JIC Germplasm Resources Unit
613 for providing the wheat TILLING lines. We also thank three anonymous reviewers for their
614 helpful comments that improved this manuscript.

615

616

617 **AUTHOR CONTRIBUTION**

618 EH and DS conceived and led the study, and designed most of the experiments. EH
619 conducted most of the experiments. JC designed and conducted the Arabidopsis
620 complementation experiments. AWL designed and conducted the transcriptomics analyses.
621 JAJ and FW designed and conducted the HPLC-SEC analyses. JEB designed and conducted
622 TEM experiments and performed sectioning. BF designed and conducted the crosses of the
623 wheat TILLING lines. MH designed the analysis of the granule size distribution data. All
624 authors analysed data. EH and DS wrote the paper with contributions from all authors.

625

626 **REFERENCES**

- 627 **Abt MR, Pfister B, Sharma M, Eicke S, Bürgy L, Neale I, Seung D, Zeeman SC. 2020.** STARCH
628 SYNTHASE5, a Noncanonical Starch Synthase-Like Protein, Promotes Starch Granule
629 Initiation in Arabidopsis. *The Plant Cell* **32**: 2543–2565.
- 630 **Abt MR, Zeeman SC. 2020.** Evolutionary innovations in starch metabolism. *Current Opinion*
631 *in Plant Biology* **55**: 109–117.
- 632 **Appels R, Eversole K, Stein N, Feuillet C, Keller B, Rogers J, Pozniak CJ, Choulet F, Distelfeld**
633 **A, Poland J, et al. 2018.** Shifting the limits in wheat research and breeding using a fully
634 annotated reference genome. *Science* **361**: eaar7191.
- 635 **Bechtel DB, Zayas I, Kaleikau L, Pomeranz Y. 1990.** Size-distribution of wheat starch
636 granules during endosperm development. *Cereal Chemistry* **67**: 59–63.
- 637 **Bolger AM, Lohse M, Usadel B. 2014.** Trimmomatic: A flexible trimmer for Illumina
638 sequence data. *Bioinformatics* **30**: 2114–2120.
- 639 **Borrill P, Ramirez-Gonzalez R, Uauy C. 2016.** expVIP: a Customizable RNA-seq Data Analysis
640 and Visualization Platform. *Plant Physiology* **170**: 2172–2186.
- 641 **Brust H, Orzechowski S, Fettke J, Steup M. 2013.** Starch synthesizing reactions and paths: in
642 vitro and in vivo studies. *Journal of Applied Glycoscience* **60**: 3–20.
- 643 **Burton RA, Jenner H, Carrangis L, Fahy B, Fincher GB, Hylton C, Laurie DA, Parker M, Waite**
644 **D, Van Wegen S, et al. 2002.** Starch granule initiation and growth are altered in barley
645 mutants that lack isoamylase activity. *Plant Journal* **31**: 97–112.
- 646 **Cave R, Seabrook S, Gidley M, Gilbert R. 2009.** Characterization of starch by size-exclusion
647 chromatography: The limitations imposed by shear scission. *Biomacromolecules* **10**: 2245–
648 2253.
- 649 **Chia T, Chirico M, King R, Ramirez-Gonzalez R, Saccomanno B, Seung D, Simmonds J, Trick**
650 **M, Uauy C, Verhoeven T, et al. 2020.** A carbohydrate-binding protein, B-GRANULE
651 CONTENT 1, influences starch granule size distribution in a dose-dependent manner in
652 polyploid wheat. *Journal of Experimental Botany* **71**: 105–115.
- 653 **Clavijo BJ, Venturini L, Schudoma C, Accinelli GG, Kaithakottil G, Wright J, Borrill P,**
654 **Kettleborough G, Heavens D, Chapman H, et al. 2017.** An improved assembly and
655 annotation of the allohexaploid wheat genome identifies complete families of agronomic
656 genes and provides genomic evidence for chromosomal translocations. *Genome Research*
657 **27**: 885–896.

- 658 **Crumpton-Taylor M, Grandison S, Png KMY, Bushby AJ, Smith AM. 2012.** Control of starch
659 granule numbers in Arabidopsis chloroplasts. *Plant Physiology* **158**: 905–916.
- 660 **Crumpton-Taylor M, Pike M, Lu KJ, Hylton CM, Feil R, Eicke S, Lunn JE, Zeeman SC, Smith**
661 **AM. 2013.** Starch synthase 4 is essential for coordination of starch granule formation with
662 chloroplast division during Arabidopsis leaf expansion. *New Phytologist* **200**: 1064–1075.
- 663 **Cuesta-Seijo JA, Nielsen MM, Ruzanski C, Krucewicz K, Beeren SR, Rydhal MG, Yoshimura**
664 **Y, Striebeck A, Motawia MS, Willats WGT, et al. 2016.** In vitro biochemical characterization
665 of all barley endosperm starch synthases. *Frontiers in Plant Science* **6**: 1–17.
- 666 **Delatte T, Trevisan M, Parker ML, Zeeman SC. 2005.** Arabidopsis mutants Atisa1 and Atisa2
667 have identical phenotypes and lack the same multimeric isoamylase, which influences the
668 branch point distribution of amylopectin during starch synthesis. *Plant Journal* **41**: 815–830.
- 669 **Delvallé D, Dumez S, Wattebled F, Roldán I, Planchot V, Berbezy P, Colonna P, Vyas D,**
670 **Chatterjee M, Ball S, et al. 2005.** Soluble starch synthase I: a major determinant for the
671 synthesis of amylopectin in Arabidopsis thaliana leaves. *Plant Journal* **43**: 398–412.
- 672 **Dumez S, Wattebled F, Dauvillee D, Delvalle D, Planchot V, Ball SG, D’Hulst C. 2006.**
673 Mutants of Arabidopsis lacking starch branching enzyme II substitute plastidial starch
674 synthesis by cytoplasmic maltose accumulation. *Plant Cell* **18**: 2694–2709.
- 675 **Fujita N, Yoshida M, Asakura N, Ohdan T, Miyao A, Hirochika H, Nakamura Y. 2006.**
676 Function and characterization of starch synthase I using mutants in rice. *Plant Physiology*
677 **140**: 1070–1084.
- 678 **Fujita N, Yoshida M, Kondo T, Saito K, Utsumi Y, Tokunaga T, Nishi A, Satoh H, Park JH,**
679 **Jane JL, et al. 2007.** Characterization of SSIIIa-deficient mutants of rice: the function of SSIIIa
680 and pleiotropic effects by SSIIIa deficiency in the rice endosperm. *Plant Physiology* **144**:
681 2009–2023.
- 682 **Grefen C, Donald N, Hashimoto K, Kudla J, Schumacher K, Blatt MR. 2010.** A ubiquitin-10
683 promoter-based vector set for fluorescent protein tagging facilitates temporal stability and
684 native protein distribution in transient and stable expression studies. *Plant Journal* **64**: 355–
685 365.
- 686 **Guo H, Liu Y, Li X, Yan Z, Xie Y, Xiong H, Zhao L, Gu J, Zhao S, Liu L. 2017.** Novel mutant
687 alleles of the starch synthesis gene TaSSIVb-D result in the reduction of starch granule
688 number per chloroplast in wheat. *BMC Genomics* **18**: 1–10.
- 689 **Howard T, Rejab NA, Griffiths S, Leigh F, Leverington-Waite M, Simmonds J, Uauy C,**

- 690 **Trafford K. 2011.** Identification of a major QTL controlling the content of B-type starch
691 granules in *Aegilops*. *Journal of Experimental Botany* **62**: 2217–2228.
- 692 **Hwang S-K, Nishi A, Satoh H, Okita TW. 2010.** Rice endosperm-specific plastidial alpha-
693 glucan phosphorylase is important for synthesis of short-chain malto-oligosaccharides.
694 *Archives of biochemistry and biophysics* **495**: 82–92.
- 695 **Irshad, Guo, Zhang, Gu, Zhao, Xie, Xiong, Zhao, Ding, Ma, et al. 2019.** EcoTILLING reveals
696 natural allelic variations in starch synthesis key gene TaSSIV and its haplotypes associated
697 with higher thousand grain weight. *Genes* **10**: 307.
- 698 **Jung YJ, Nogoy FM, Lee SK, Cho YG, Kang KK. 2018.** Application of ZFN for site directed
699 mutagenesis of rice SSIVa gene. *Biotechnology and Bioprocess Engineering* **23**: 108–115.
- 700 **Karimi M, Inzé D, Depicker A. 2002.** GATEWAY vectors for *Agrobacterium*-mediated plant
701 transformation. *Trends in plant science* **7**: 193–195.
- 702 **Kawagoe Y. 2013.** The characteristic polyhedral, sharp-edged shape of compound-type
703 starch granules in rice endosperm is achieved via the septum-like structure of the
704 amyloplast. *Journal of Applied Glycoscience* **60**: 29–36.
- 705 **Kersey PJ, Allen JE, Allot A, Barba M, Boddu S, Bolt BJ, Carvalho-Silva D, Christensen M,
706 Davis P, Grabmueller C, et al. 2018.** Ensembl Genomes 2018: An integrated omics
707 infrastructure for non-vertebrate species. *Nucleic Acids Research* **46**: D802–D808.
- 708 **Krasileva K V., Vasquez-Gross HA, Howell T, Bailey P, Paraiso F, Clissold L, Simmonds J,
709 Ramirez-Gonzalez RH, Wang X, Borrill P, et al. 2017.** Uncovering hidden variation in
710 polyploid wheat. *Proceedings of the National Academy of Sciences* **114**: E913–E921.
- 711 **Langeveld SMJ, Van wijk R, Stuurman N, Kijne JW, de Pater S. 2000.** B-type granule
712 containing protrusions and interconnections between amyloplasts in developing wheat
713 endosperm revealed by transmission electron microscopy and GFP expression. *Journal of*
714 *Experimental Botany* **51**: 1357–1361.
- 715 **Lee SK, Eom JS, Hwang SK, Shin D, An G, Okita TW, Jeon JS. 2016.** Plastidic
716 phosphoglucomutase and ADP-glucose pyrophosphorylase mutants impair starch synthesis
717 in rice pollen grains and cause male sterility. *Journal of Experimental Botany* **67**: 5557–5569.
- 718 **Lu K-J, Pfister B, Jenny C, Eicke S, Zeeman SC. 2018.** Distinct functions of STARCH SYNTHASE
719 4 domains in starch granule formation. *Plant Physiology* **176**: 566–581.
- 720 **Maccaferri M, Harris NS, Twardziok SO, Pasam RK, Gundlach H, Spannagl M,
721 Ormanbekova D, Lux T, Prade VM, Milner SG, et al. 2019.** Durum wheat genome highlights

722 past domestication signatures and future improvement targets. *Nature Genetics* **51**: 885–
723 895.

724 **Matsushima R, Maekawa M, Sakamoto W. 2015.** Geometrical formation of compound
725 starch grains in rice implements Voronoi diagram. *Plant and Cell Physiology* **56**: 2150–2157.

726 **Matsushima R, Yamashita J, Kariyama S, Enomoto T, Sakamoto W. 2013.** A phylogenetic
727 re-evaluation of morphological variations of starch grains among Poaceae species. *Journal of*
728 *Applied Glycoscience* **60**: 131–135.

729 **Morell MK, Kosar-Hashemi B, Cmiel M, Samuel MS, Chandler P, Rahman S, Buleon A,**
730 **Batey IL, Li Z. 2003.** Barley sex6 mutants lack starch synthase IIa activity and contain a starch
731 with novel properties. *Plant Journal* **34**: 173–185.

732 **Parker ML. 1985.** The relationship between A-type and B-type starch granules in the
733 developing endosperm of wheat. *Journal of Cereal Science* **3**: 271–278.

734 **Patro R, Duggal G, Love MI, Irizarry RA, Kingsford C. 2017.** Salmon provides fast and bias-
735 aware quantification of transcript expression. *Nature Methods* **14**: 417–419.

736 **Peng C, Wang Y, Liu F, Ren Y, Zhou K, Lv J, Zheng M, Zhao S, Zhang L, Wang C, et al. 2014.**
737 FLOURY ENDOSPERM6 encodes a CBM48 domain-containing protein involved in compound
738 granule formation and starch synthesis in rice endosperm. *Plant Journal* **77**: 917–930.

739 **Ragel P, Streb S, Feil R, Sahrawy M, Annunziata MG, Lunn JE, Zeeman S, Mérida Á. 2013.**
740 Loss of starch granule initiation has a deleterious effect on the growth of Arabidopsis plants
741 due to an accumulation of ADP-glucose. *Plant Physiology* **163**: 75–85.

742 **Roldán I, Wattebled F, Mercedes Lucas M, Delvallé D, Planchot V, Jiménez S, Pérez R, Ball**
743 **S, D’Hulst C, Mérida A. 2007.** The phenotype of soluble starch synthase IV defective
744 mutants of Arabidopsis thaliana suggests a novel function of elongation enzymes in the
745 control of starch granule formation. *Plant Journal* **49**: 492–504.

746 **Saito M, Tanaka T, Sato K, Vrinten P, Nakamura T. 2017.** A single nucleotide polymorphism
747 in the “Fra” gene results in fractured starch granules in barley. *Theoretical and Applied*
748 *Genetics* **131**: 353–364.

749 **Seung D. 2020.** Amylose in starch: towards an understanding of biosynthesis, structure and
750 function. *New Phytologist In Press*: nph.16858.

751 **Seung D, Boudet J, Monroe JD, Schreier TB, David LC, Abt M, Lu K-J, Zanella M, Zeeman SC.**
752 **2017.** Homologs of PROTEIN TARGETING TO STARCH control starch granule initiation in
753 Arabidopsis leaves. *Plant Cell* **29**: 1657–1677.

- 754 **Seung D, Lu K-J, Stettler M, Streb S, Zeeman SC. 2016.** Degradation of glucan primers in the
755 absence of Starch Synthase 4 disrupts starch granule initiation in *Arabidopsis*. *Journal of*
756 *Biological Chemistry* **291**: 20718–20728.
- 757 **Seung D, Schreier TB, Bürgy L, Eicke S, Zeeman SC. 2018.** Two plastidial coiled-coil proteins
758 are essential for normal starch granule initiation in *Arabidopsis*. *Plant Cell* **30**: 1523–1542.
- 759 **Seung D, Smith A. 2019.** Starch granule initiation and morphogenesis – progress in
760 *Arabidopsis* and cereals. *Journal of Experimental Botany* **70**: 771–784.
- 761 **Seung D, Soyk S, Coiro M, Maier BA, Eicke S, Zeeman SC. 2015.** PROTEIN TARGETING TO
762 STARCH is required for localising GRANULE-BOUND STARCH SYNTHASE to starch granules
763 and for normal amylose synthesis in *Arabidopsis*. *PLOS Biology* **13**: e1002080.
- 764 **Smith AM, Zeeman SC. 2020.** Starch: A flexible, adaptable carbon store coupled to plant
765 growth. *Annual Review of Plant Biology* **71**: 217–245.
- 766 **Suh DS, Verhoeven T, Denyer K, Jane JL. 2004.** Characterization of Nubet and Franubet
767 barley starches. *Carbohydrate Polymers* **56**: 85–93.
- 768 **Sundberg M, Pfister B, Fulton D, Bischof S, Delatte T, Eicke S, Stettler M, Smith SM, Streb**
769 **S, Zeeman SC. 2013.** The heteromultimeric debranching enzyme involved in starch synthesis
770 in *Arabidopsis* requires both Isoamylase1 and Isoamylase2 subunits for complex stability
771 and activity. *PLOS One* **8**: e75223.
- 772 **Szydłowski N, Ragel P, Hennen-Bierwagen T a, Planchot V, Myers AM, Mérida A, D’Hulst C,**
773 **Wattebled F. 2011.** Integrated functions among multiple starch synthases determine both
774 amylopectin chain length and branch linkage location in *Arabidopsis* leaf starch. *Journal of*
775 *Experimental Botany*: 1–13.
- 776 **Szydłowski N, Ragel P, Raynaud S, Lucas MM, Roldán I, Montero M, Muñoz FJ, Ovecka M,**
777 **Bahaji A, Planchot V, et al. 2009.** Starch granule initiation in *Arabidopsis* requires the
778 presence of either class IV or class III starch synthases. *Plant Cell* **21**: 2443–2457.
- 779 **Tanaka E, Ral JPF, Li S, Gaire R, Cavanagh CR, Cullis BR, Whan A. 2017.** Increased accuracy
780 of starch granule type quantification using mixture distributions. *Plant Methods*: 1–7.
- 781 **Toyosawa Y, Kawagoe Y, Matsushima R, Crofts N, Ogawa M, Fukuda M, Kumamaru T,**
782 **Okazaki Y, Kusano M, Saito K, et al. 2016.** Deficiency of starch synthase IIIa and IVb alters
783 starch granule morphology from polyhedral to spherical in rice endosperm. *Plant Physiology*
784 **170**: 1255–1270.
- 785 **Tuncel A, Corbin KR, Ahn-Jarvis J, Harris S, Hawkins E, Smedley MA, Harwood W, Warren**

786 **FJ, Patron NJ, Smith AM. 2019.** Cas9-mediated mutagenesis of potato starch-branching
787 enzymes generates a range of tuber starch phenotypes. *Plant Biotechnology Journal* **17**:
788 2259–2271.

789 **Vandromme C, Spriet C, Dauvillée D, Courseaux A, Putaux J, Wychowski A, Krzewinski F,**
790 **Facon M, D’Hulst C, Wattebled F. 2019.** PII1: a protein involved in starch initiation that
791 determines granule number and size in Arabidopsis chloroplast. *New Phytologist* **221**: 356–
792 370.

793 **Vilaplana F, Hasjim J, Gilbert RG. 2012.** Amylose content in starches: Toward optimal
794 definition and validating experimental methods. *Carbohydrate Polymers* **88**: 103–111.

795 **Wang YJ, White P, Pollak L, Jane J. 1993.** Characterization of starch structures of 17 maize
796 endosperm mutant genotypes with Oh43 inbred line background. *Cereal Chemistry* **70**: 171–
797 179.

798 **Wu AC, Li E, Gilbert RG. 2014.** Exploring extraction/dissolution procedures for analysis of
799 starch chain-length distributions. *Carbohydrate Polymers* **114**: 36–42.

800 **Xiang D, Quilichini TD, Liu Z, Gao P, Pan Y, Li Q, Nilsen KT, Venglat P, Esteban E, Pasha A, et**
801 **al. 2019.** The transcriptional landscape of polyploid wheats and their diploid ancestors
802 during embryogenesis and grain development[OPEN]. *Plant Cell* **31**: 2888–2911.

803 **Yun MS, Kawagoe Y. 2010.** Septum formation in amyloplasts produces compound granules
804 in the rice endosperm and is regulated by plastid division proteins. *Plant and Cell Physiology*
805 **51**: 1469–1479.

806 **Zhang X, Henriques R, Lin S-S, Niu Q-W, Chua N-H. 2006.** Agrobacterium-mediated
807 transformation of Arabidopsis thaliana using the floral dip method. *Nature protocols* **1**: 641–
808 6.

809 **Zhang X, Myers A, James M. 2005.** Mutations affecting starch synthase III in Arabidopsis
810 alter leaf starch structure and increase the rate of starch synthesis. *Plant Physiology* **138**:
811 663–674.

812 **Zhang X, Szydlowski N, Delvallé D, D’Hulst C, James MG, Myers AM. 2008.** Overlapping
813 functions of the starch synthases SSII and SSIII in amylopectin biosynthesis in Arabidopsis.
814 *BMC Plant Biology* **8**: 96.

815

816 **FIGURE LEGENDS**

817

818 **Fig. 1. Schematic illustrations of *TaSS4* homoeologs.** (a) Location of *TaSS4* homoeologs on
819 group 1 chromosomes. The red boxes represent *TaSS4* homoeologs, while homoeologs of
820 the adjacent genes are shown in green (phosphodiesterase-like protein), purple (glycoside
821 hydrolase family 18 protein), blue (P loop-containing nucleoside triphosphate hydrolase)
822 and orange (serine acetyltransferase-like protein). Arrowheads on the boxes indicate
823 direction of transcription. Chromosome coordinates are indicated below each region. (b)
824 Gene models of the *TaSS4* homoeologs. Exons are represented with blue boxes, while light
825 blue boxes represent the 5' and 3' UTRs. Mutations in the *Tass4-1* and *Tass4-2* mutant lines
826 are depicted with red arrows and the mutated codons/amino acids are shown in red letters.
827 The polymorphism in *TaSS4-1A* between Kronos and Chinese Spring (CS) is indicated.

828

829 **Fig. 2. *TaSS4* and *TaBGC1* protein levels in developing endosperm.** (a) Total proteins were
830 extracted from developing endosperms at 10, 15 and 20 dpa, and immunoblotted using
831 anti-*TaSS4* (upper panel), anti-*TaBGC1* (middle panel) or anti-actin (lower panel) antibodies.
832 Lanes were loaded on an equal protein basis. The migration of molecular weight markers
833 are indicated in kilodaltons (kDa) to the left of each panel. Two replicate extractions for
834 each genotype (numbered 1 and 2) were prepared from grains harvested from two different
835 plants. (b) Same as (a), but with *Tass4-1* grains harvested at 10 dpa. (c) Same as (a), but with
836 *Tabgc1* grains harvested at 20 dpa.

837

838 **Fig. 3. *Tass4-1* double mutants have severely altered granule morphology.** (a) Endosperm
839 starch granules from mature grains were observed using scanning electron microscopy.
840 Single (*aa BB* or *AA bb*) and double mutants (*aa bb*) were compared with control (*AA BB*)
841 lines. Bars = 10 μ m. (b) As (a), but granules were observed using cross-polarised light
842 microscopy. The multiple hila in the large polyhedral granule are indicated with red arrows.
843 Bars = 10 μ m. (c) Size distribution of endosperm starch granules. The volume of granules at
844 each diameter relative to the total granule volume was quantified using a Coulter counter.
845 Values represent mean (solid line) \pm SEM (shading) of three replicate starch extractions from
846 grains of three different plants.

847

848 **Fig. 4. Aberrant granules in *Tass4-1* double mutants form early in grain development.** (a)
849 Endosperm starch from developing grains (8, 14 and 21 dpa) of the *Tass4-1* double mutant
850 (*aa bb*) and control lines (*AA BB*) were observed using scanning electron microscopy. Bars =
851 25 μ m. (b) Size distribution of endosperm starch granules. The volume of granules at each
852 diameter relative to the total granule volume was quantified using a Coulter counter. Values
853 represent mean (solid line) \pm SEM (shading) of three replicate starch extractions from grains
854 of three different plants, except for *aa bb* at 8 dpa where one starch extraction was
855 performed.

856

857 **Fig. 5. Endosperm sections of *Tass4-1* single and double mutants.** (a) Thin sections were
858 prepared from mature grains, stained with iodine and observed using light microscopy.
859 Single (*aa BB* or *AA bb*) and double mutants (*aa bb*) were compared with control (*AA BB*)
860 lines. Bars = 25 μ m. (b) Insets showing a close-up view of a large compound structure (left
861 panel) and a tubule-like structure (right panel) in the *aa bb* section – both indicated with red
862 arrows. Bars = 25 μ m.

863

864 **Fig. 6. Compound granules in the developing *Tass4-1* endosperm. (a)** Toluidine blue-
865 stained sections of developing endosperm (15 dpa) in the *Tass4-1* double mutant (*aa bb*) or
866 control (AA BB), observed using light microscopy. Blue arrows indicate examples of normal
867 A-type granules, while red arrows indicate compound granules. Bars = 20 μ m. **(b)** Same as
868 **(a)**, but observed using transmission electron microscopy. Amyloplast membranes and
869 stromal space around granules are indicated with yellow arrows. Bars = 5 μ m.

870

871 **Fig. 7. Similar defects in granule morphology in *Tass4* and *Tabgc1* mutants. (a)** Gene
872 models of the *TabGC1* homoeologs. Exons are represented with blue boxes, while light blue
873 boxes represent the 5' and 3' UTRs. The locations of the mutations in the *Tabgc1-3* and
874 *Tabgc1-4* lines are depicted with red arrows and the mutated codons/amino acids are
875 shown in red letters. **(b)** Purified starch granules from mature grains of the double mutants
876 (*aa bb*) and control lines (AA BB) observed using scanning electron microscopy. Examples of
877 polyhedral granules are marked with red arrows. Bars = 10 μ m. **(c)** Size distribution of
878 endosperm starch granules in mature grains of the *Tabgc1-3* single (*aa BB* and AA *bb*) and
879 double mutants. The volume of granules at each diameter relative to the total granule
880 volume was quantified using a Coulter counter. Values represent mean (solid line) \pm SEM
881 (shading) of three replicate starch extractions from grains of three different plants. **(d)** Same
882 as **(c)**, but with *Tabgc1-4*.

883

884 **Fig. 8. Growth and fertility phenotypes of the *Tass4* mutant. (a)** Photograph of 8-week old
885 plants of wild type, *Tass4-1* control (AA BB) and double mutant (*aa bb*). **(b)** Photographs of
886 mature grains. **(c)** The number of tillers on backcrossed (BC₂F₂) and non-backcrossed *Tass4-1*
887 mutants were counted on $n=5-7$ plants. Individual data points (black dots) and the mean
888 (red dot) are shown over the box plots. There were no significant differences between the
889 lines under a one-way ANOVA. **(d)** The average number of grains in the three primary spikes
890 was calculated for $n=5-7$ plants. Plots are as for **(c)**. Different letters indicate significant
891 differences at $p < 0.05$ under a one-way ANOVA and Tukey's posthoc test. Note that the
892 statistical analysis includes data in Fig. S8c, which were obtained in the same experiment.
893 **(e)** Iodine-stained pollen grains observed with light microscopy. Bars = 50 μ m.

894

895 **Fig. 9. Loss of *TaSS4* results in fewer starch granules in leaf chloroplasts. (a)** Leaf starch
896 content at the end of day. Bars represent the mean \pm SEM from $n = 10$ plants. Different
897 letters indicate significant differences at $p < 0.05$ under a one-way ANOVA and Tukey's
898 posthoc test. **(b)** Starch granules in mesophyll chloroplasts observed with light microscopy.
899 Leaf samples were harvested at the end of day from the middle of the flag leaf of 5-week
900 old plants. Thin sections were stained with toluidine blue and periodic acid/Schiff's reagent.
901 Bars = 10 μ m. **(c)** Quantification of starch granule number per chloroplast. Three replicate
902 sections for each genotype (each produced from separate plants, plotted as black, dark grey
903 and light grey bars) were observed using light microscopy as in **(b)** (except for *aa BB*, where
904 two replicate sections were produced). Histograms represent the frequency of chloroplast
905 sections containing a given number of granule sections, relative to the total number of
906 chloroplast sections. A total of 217-237 chloroplasts were analysed for each replicate. **(d)**
907 Leaf chloroplasts were imaged using transmission electron microscopy. Bars = 2 μ m.

908

909 **Fig. 10. *TaSS4* can partially complement plant growth and starch granule morphology**
910 **phenotypes of the *Arabidopsis Atss4* mutant. (a)** Rosette morphology of the wild type (Col-
911 0), *Atss4* mutant, and two independent transgenic lines expressing *TaSS4* 1B-YFP under the
912 *Arabidopsis Ubiquitin10* promoter in the *Atss4* mutant background (*ss4/pUBQ:TaSS4-YFP*).
913 **(b)** Starch granules in chloroplasts observed using light microscopy for the plants shown in
914 **(a)**. Thin sections of young leaves of a 5- to 6-week old rosette were stained using toluidine
915 blue and periodic acid/Schiff's reagent. Bars = 10 μ m. **(c)** Same as **(b)**, but viewed under
916 transmission electron microscopy. Bars = 2 μ m.

917
918 **Fig. 11. Model of *TaSS4* action in endosperm starch initiation.** *TaSS4* and *TaBGC1* are
919 required for the control of normal A-type granule initiation. We propose that they establish
920 a single granule initial that serves as the preferred substrate of other biosynthesis
921 enzymes for building an A-type granule. In the absence of the granule initial, the other biosynthesis
922 enzymes begin to elongate other available substrates such as soluble maltooligosaccharides,
923 which results in the initiation of an undefined number of granules. This leads to
924 heterogeneity among amyloplasts, where most have multiple initiations (leading to a
925 compound granule) and some have normal A-type granules. It is possible that some
926 amyloplasts do not initiate any starch granule, but the prevalence of this is unknown.
927 Abbreviations are SS – starch synthase, PHS – starch phosphorylase, BE – branching enzyme,
928 DBE – debranching enzyme.
929

930 **Table 1: Starch content, composition and granule size in *Tass4-1* mature grains.**

Genotype	Starch content (% flour weight)	Amylose content (% starch)	A-type granule mean diameter (μm)	B-type granule mean diameter (μm)	B-type granule volume (%)
AA BB	50 \pm 3	31 \pm 2	19.1 \pm 0.7	7.9 \pm 0.9	38.1 \pm 2.2
<i>aa</i> BB	59 \pm 4	32 \pm 2	18.9 \pm 0.4	6.7 \pm 0.1	39.8 \pm 0.8
AA <i>bb</i>	51 \pm 5	32 \pm 3	20.5 \pm 0.3	7.4 \pm 0.1	37.9 \pm 0.8
<i>aa bb</i>	42 \pm 2	30 \pm 1	-	-	-

931 Starch content was determined as glucose equivalents and is expressed as a percentage of
932 the flour weight. Amylose content of starch was determined by HPLC-SEC. The mean
933 diameters of A-type and B-type granules and the relative volume of B-type granules were
934 determined using a Coulter counter. All values are mean \pm S.E from $n = 3$ biological
935 replicates, defined as grains harvested from three different plants. There were no significant
936 differences between any of the lines in any of these parameters under a one-way ANOVA at
937 $p < 0.05$.

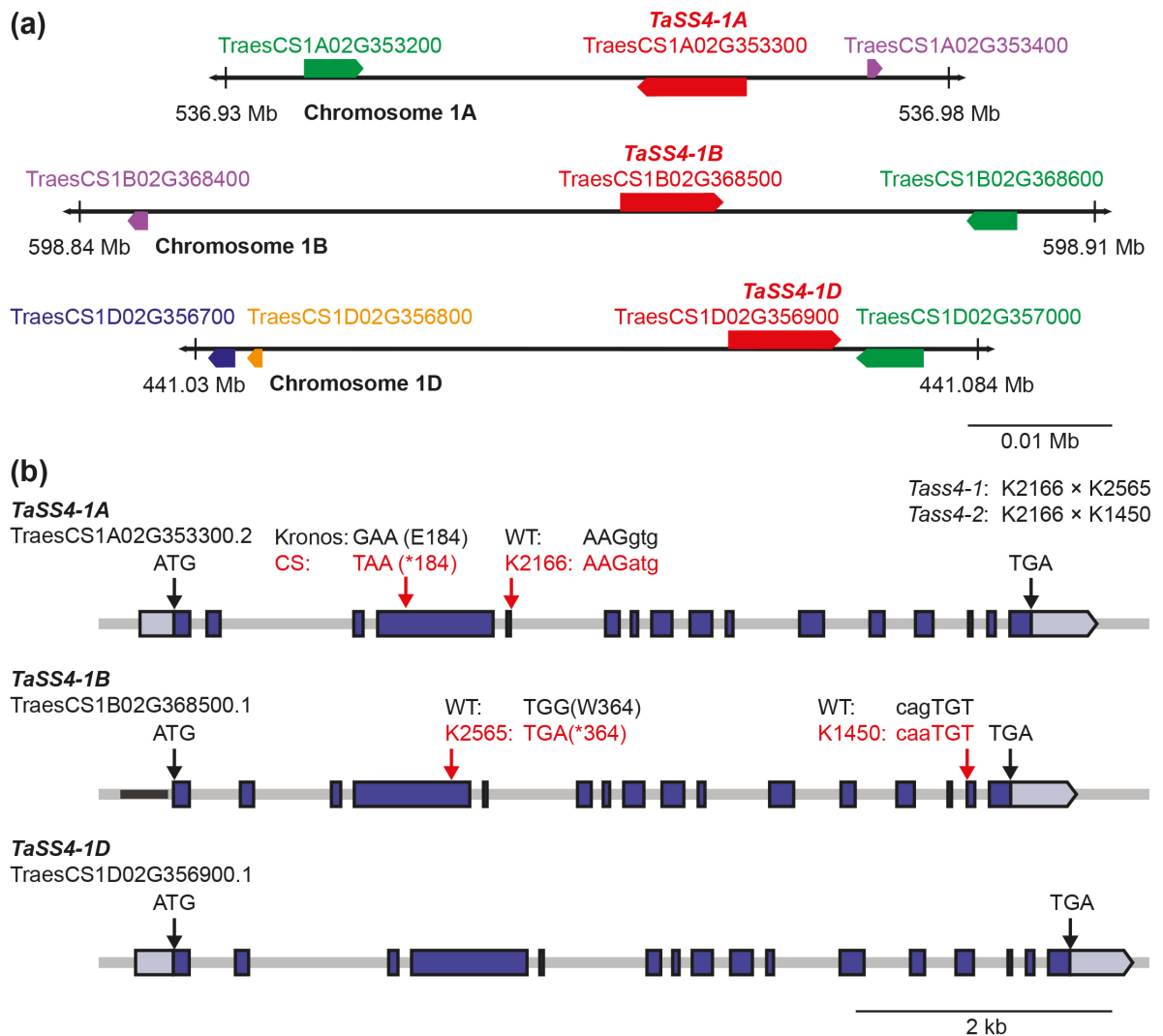


Fig. 1. Schematic illustrations of *TaSS4* homoeologs. (a) Location of *TaSS4* homoeologs on group 1 chromosomes. The red boxes represent *TaSS4* homoeologs, while homoeologs of the adjacent genes are shown in green (phosphodiesterase-like protein), purple (glycoside hydrolase family 18 protein), blue (P loop-containing nucleoside triphosphate hydrolase) and orange (serine acetyltransferase-like protein). Arrowheads on the boxes indicate direction of transcription. Chromosome coordinates are indicated below each region. **(b)** Gene models of the *TaSS4* homoeologs. Exons are represented with blue boxes, while light blue boxes represent the 5' and 3' UTRs. Mutations in the *Tass4-1* and *Tass4-2* mutant lines are depicted with red arrows and the mutated codons/amino acids are shown in red letters. The polymorphism in *TaSS4-1A* between Kronos and Chinese Spring (CS) is indicated.

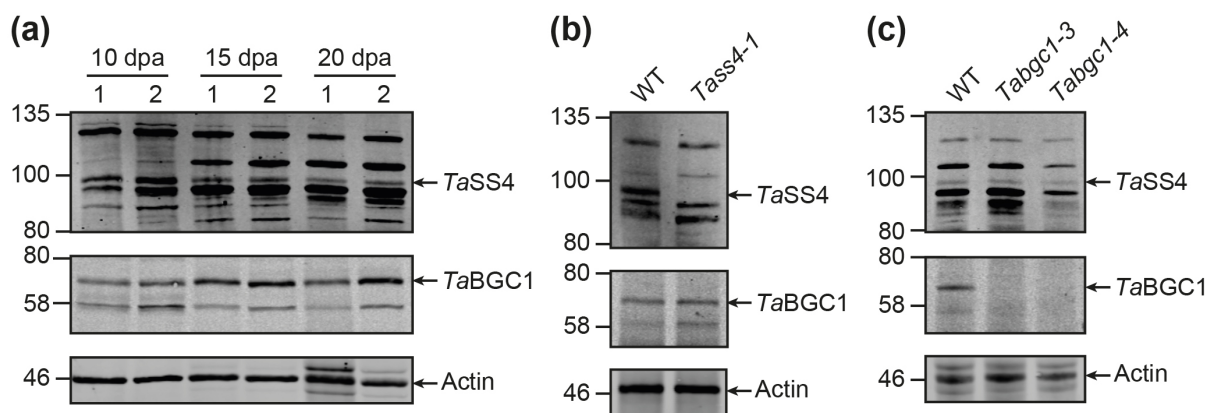


Fig. 2. *TaSS4* and *TaBGC1* protein levels in developing endosperm. (a) Total proteins were extracted from developing endosperms at 10, 15 and 20 dpa, and immunoblotted using anti-*TaSS4* (upper panel), anti-*TaBGC1* (middle panel) or anti-actin (lower panel) antibodies. Lanes were loaded on an equal protein basis. The migration of molecular weight markers are indicated in kilodaltons (kDa) to the left of each panel. Two replicate extractions for each genotype (numbered 1 and 2) were prepared from grains harvested from two different plants. (b) Same as (a), but with *Tass4-1* grains harvested at 10 dpa. (c) Same as (a), but with *Tabgc1* grains harvested at 20 dpa.

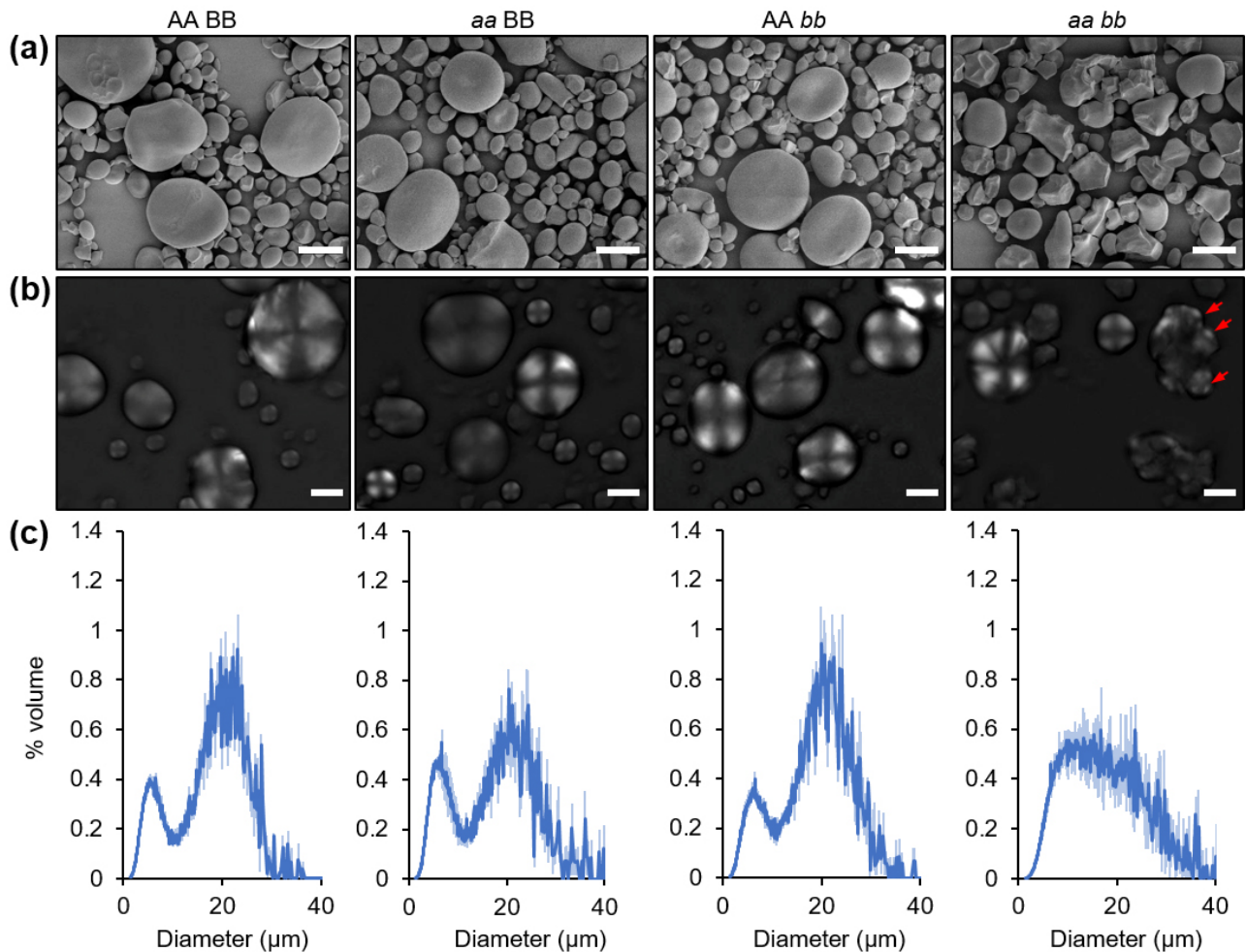


Fig. 3. *Tass4-1* double mutants have severely altered granule morphology. (a) Endosperm starch granules from mature grains were observed using scanning electron microscopy. Single (*aa BB* or *AA bb*) and double mutants (*aa bb*) were compared with control (*AA BB*) lines. Bars = 10 µm. (b) As (a), but granules were observed using cross-polarised light microscopy. The multiple hila in the large polyhedral granule are indicated with red arrows. Bars = 10 µm. (c) Size distribution of endosperm starch granules. The volume of granules at each diameter relative to the total granule volume was quantified using a Coulter counter. Values represent mean (solid line) ± SEM (shading) of three replicate starch extractions from grains of three different plants.

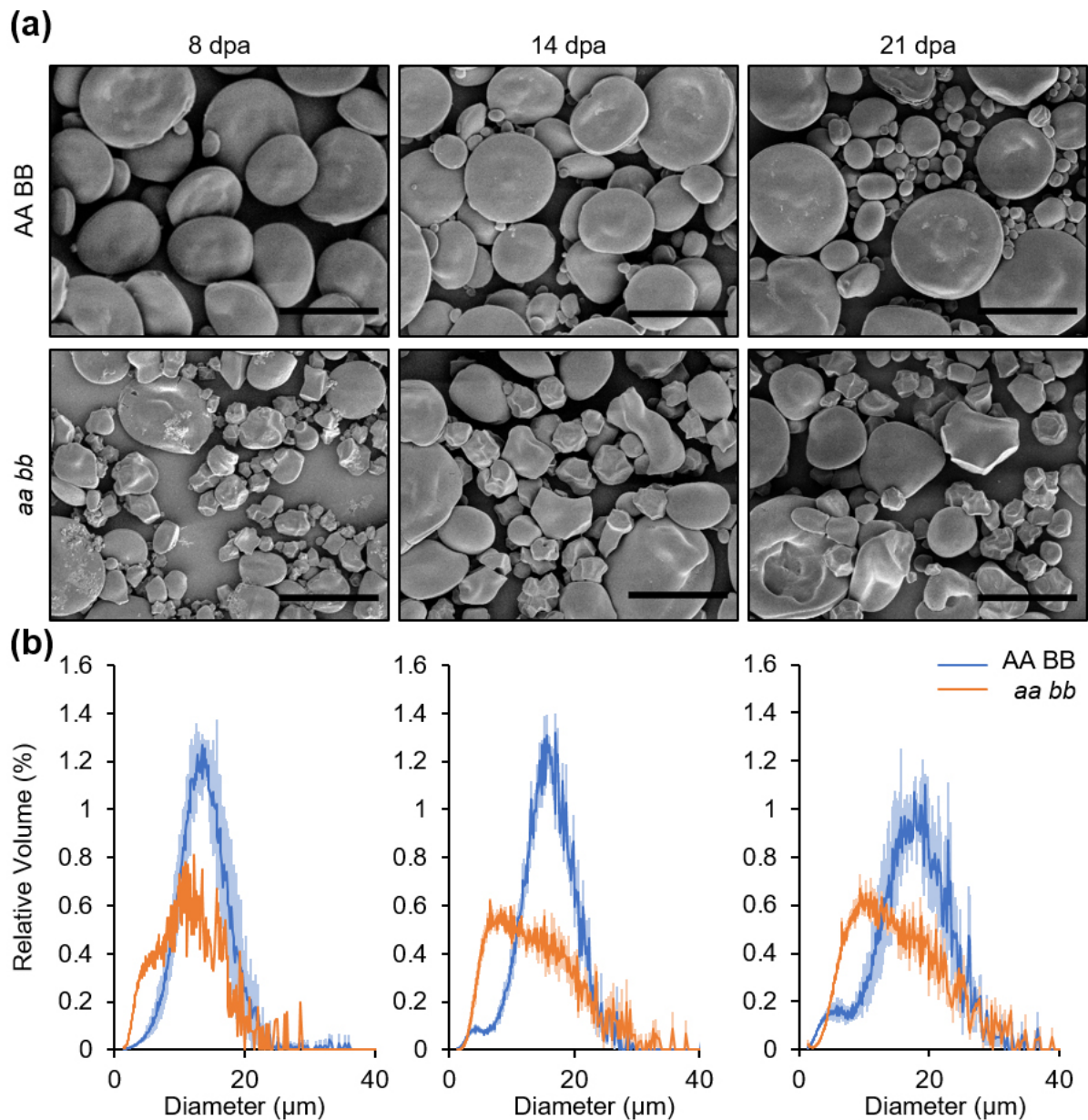


Fig. 4. Aberrant granules in *Tass4-1* double mutants form early in grain development. (a) Endosperm starch from developing grains (8, 14 and 21 dpa) of the *Tass4-1* double mutant (*aa bb*) and control lines (AA BB) were observed using scanning electron microscopy. Bars = 25 μm. (b) Size distribution of endosperm starch granules. The volume of granules at each diameter relative to the total granule volume was quantified using a Coulter counter. Values represent mean (solid line) ± SEM (shading) of three replicate starch extractions from grains of three different plants, except for *aa bb* at 8 dpa where one starch extraction was performed.

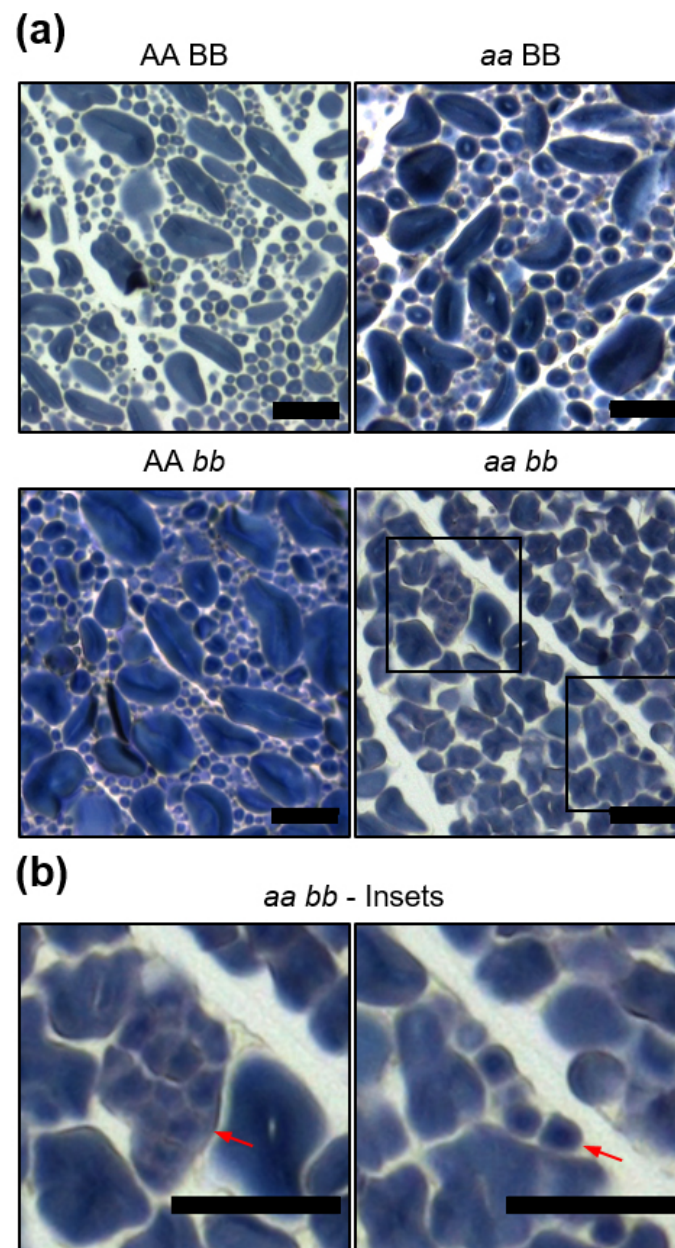


Fig. 5. Endosperm sections of *Tass4-1* single and double mutants. (a) Thin sections were prepared from mature grains, stained with iodine and observed using light microscopy. Single (*aa BB* or *AA bb*) and double mutants (*aa bb*) were compared with control (*AA BB*) lines. Bars = 25 μ m. **(b)** Insets showing a close-up view of a large compound structure (left panel) and a tubule-like structure (right panel) in the *aa bb* section – both indicated with red arrows. Bars = 25 μ m.

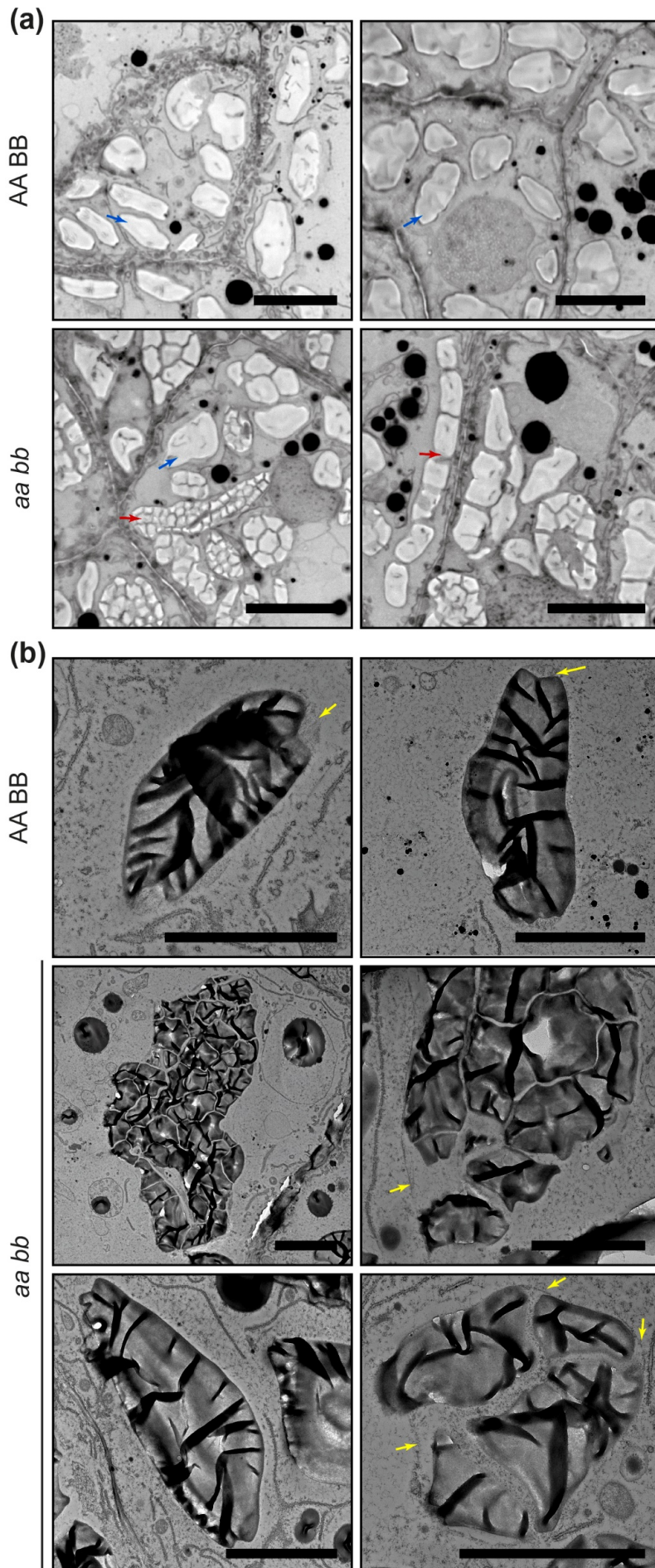


Fig. 6. Compound granules in the developing *Tass4-1* endosperm. (a) Toluidine blue-stained sections of developing endosperm (15 dpa) in the *Tass4-1* double mutant (*aa bb*) or control (AA BB), observed using light microscopy. Blue arrows indicate examples of normal A-type granules, while red arrows indicate compound granules. Bars = 20 μm. **(b)** Same as (a), but observed using transmission electron microscopy. Amyloplast membranes and stromal space around granules are indicated with yellow arrows. Bars = 5 μm.

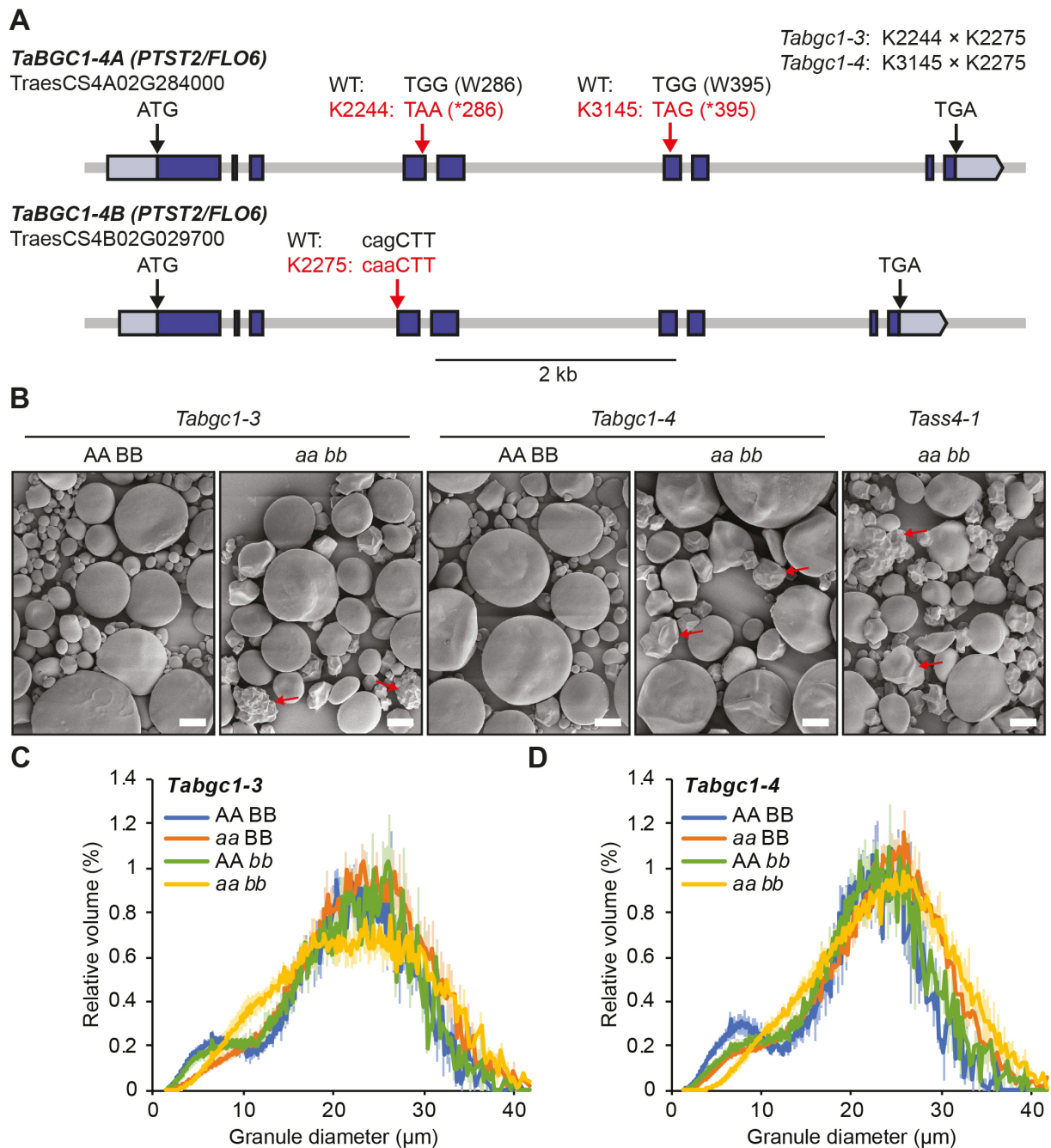


Fig. 7. Similar defects in granule morphology in *Tass4* and *Tabgc1* mutants. (a) Gene models of the *TaBGC1* homoeologs. Exons are represented with blue boxes, while light blue boxes represent the 5' and 3' UTRs. The locations of the mutations in the *Tabgc1-3* and *Tabgc1-4* lines are depicted with red arrows and the mutated codons/amino acids are shown in red letters. **(b)** Purified starch granules from mature grains of the double mutants (*aa bb*) and control lines (AA BB) observed using scanning electron microscopy. Examples of polyhedral granules are marked with red arrows. Bars = 10 μm. **(c)** Size distribution of endosperm starch granules in mature grains of the *Tabgc1-3* single (*aa BB* and AA *bb*) and double mutants. The volume of granules at each diameter relative to the total granule volume was quantified using a Coulter counter. Values represent mean (solid line) ± SEM (shading) of three replicate starch extractions from grains of three different plants. **(d)** Same as **(c)**, but with *Tabgc1-4*.

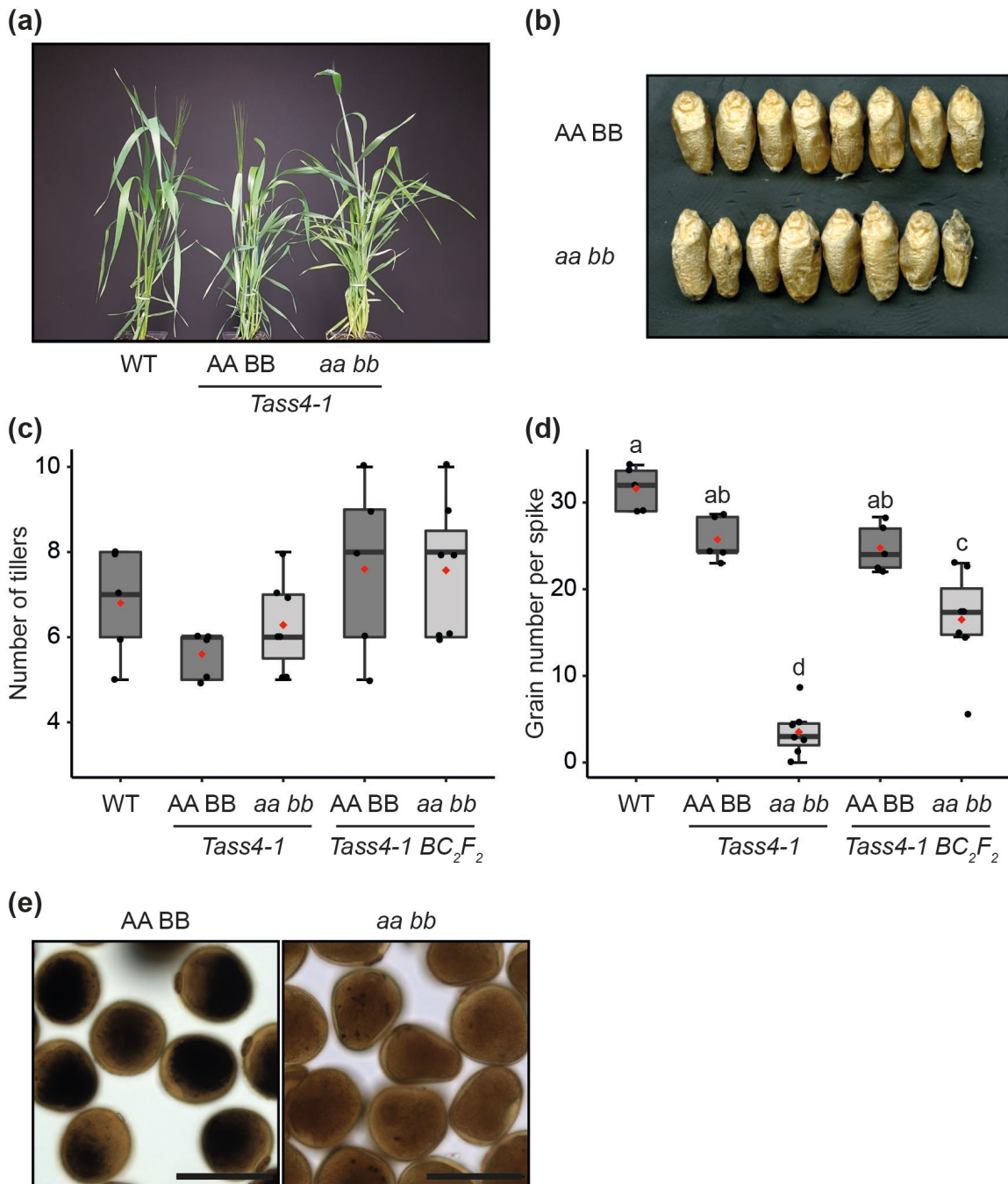


Fig. 8. Growth and fertility phenotypes of the *Tass4* mutant. **(a)** Photograph of 8-week old plants of wild type, *Tass4-1* control (AA BB) and double mutant (*aa bb*). **(b)** Photographs of mature grains. **(c)** The number of tillers on backcrossed (BC₂F₂) and non-backcrossed *Tass4-1* mutants were counted on $n=5-7$ plants. Individual data points (black dots) and the mean (red dot) are shown over the box plots. There were no significant differences between the lines under a one-way ANOVA. **(d)** The average number of grains in the three primary spikes was calculated for $n=5-7$ plants. Plots are as for **(c)**. Different letters indicate significant differences at $p < 0.05$ under a one-way ANOVA and Tukey's posthoc test. Note that the statistical analysis includes data in Fig. S8c, which were obtained in the same experiment. **(e)** Iodine-stained pollen grains observed *aa* with light microscopy. Bars = 50 μ m.

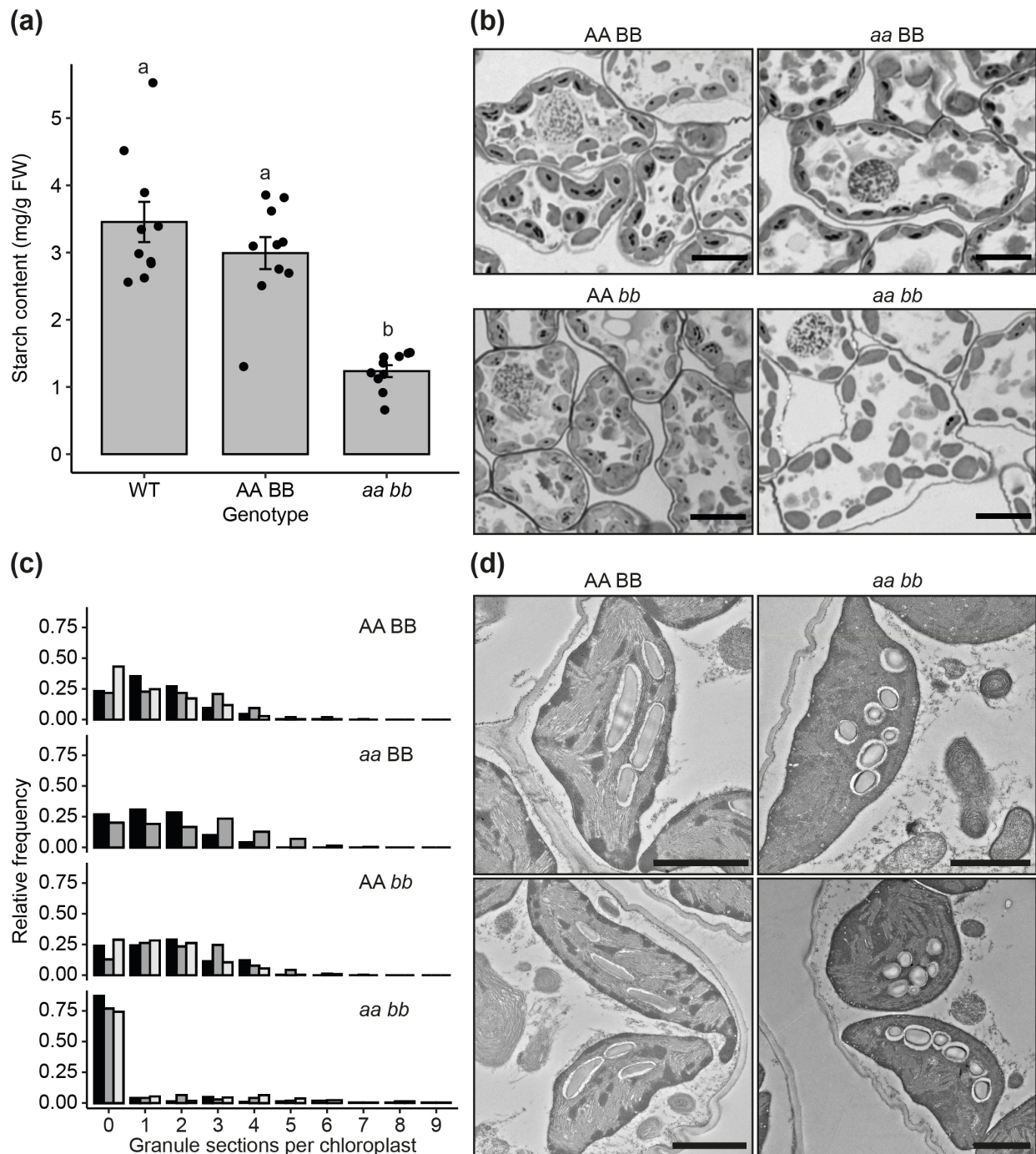


Fig. 9. Loss of *TaSS4* results in fewer starch granules in leaf chloroplasts. (a) Leaf starch content at the end of day. Bars represent the mean \pm SEM from $n = 10$ plants. Different letters indicate significant differences at $p < 0.05$ under a one-way ANOVA and Tukey's posthoc test. **(b)** Starch granules in mesophyll chloroplasts observed with light microscopy. Leaf samples were harvested at the end of day from the middle of the flag leaf of 5-week old plants. Thin sections were stained with toluidine blue and periodic acid/Schiff's reagent. Bars = 10 μ m. **(c)** Quantification of starch granule number per chloroplast. Three replicate sections for each genotype (each produced from separate plants, plotted as black, dark grey and light grey bars) were observed using light microscopy as in **(b)** (except for *aa BB*, where two replicate sections were produced). Histograms represent the frequency of chloroplast sections containing a given number of granule sections, relative to the total number of chloroplast sections. A total of 217-237 chloroplasts were analysed for each replicate. **(d)** Leaf chloroplasts were imaged using transmission electron microscopy. Bars = 2 μ m.

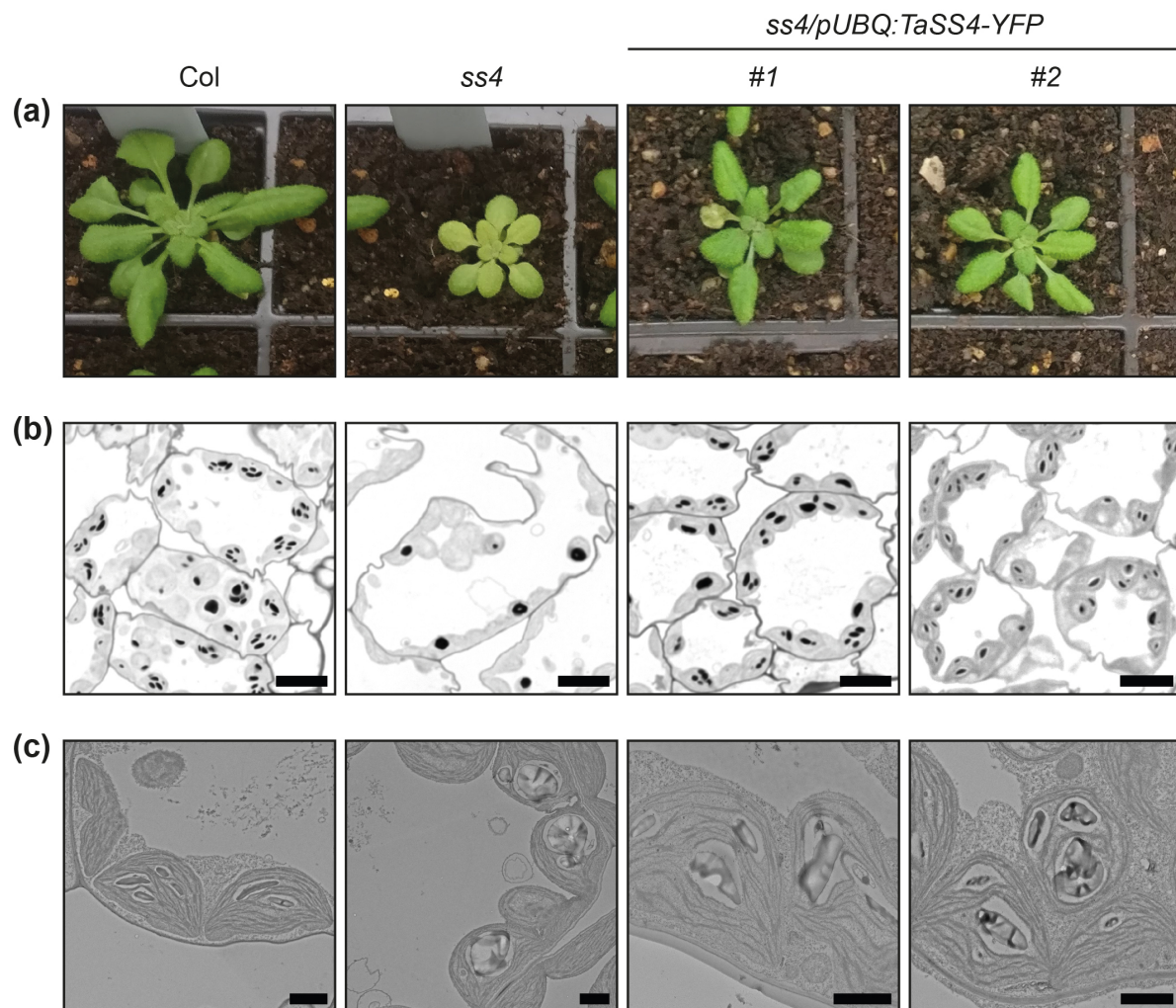


Fig. 10. *TaSS4* can partially complement plant growth and starch granule morphology phenotypes of the *Arabidopsis Atss4* mutant. (a) Rosette morphology of the wild type (Col-0), *Atss4* mutant, and two independent transgenic lines expressing *TaSS4* 1B-YFP under the *Arabidopsis Ubiquitin10* promoter in the *Atss4* mutant background (*ss4/pUBQ:TaSS4-YFP*). (b) Starch granules in chloroplasts observed using light microscopy for the plants shown in (a). Thin sections of young leaves of a 5- to 6-week old rosette were stained using toluidine blue and periodic acid/Schiff's reagent. Bars = 10 μ m. (c) Same as (b), but viewed under transmission electron microscopy. Bars = 2 μ m.

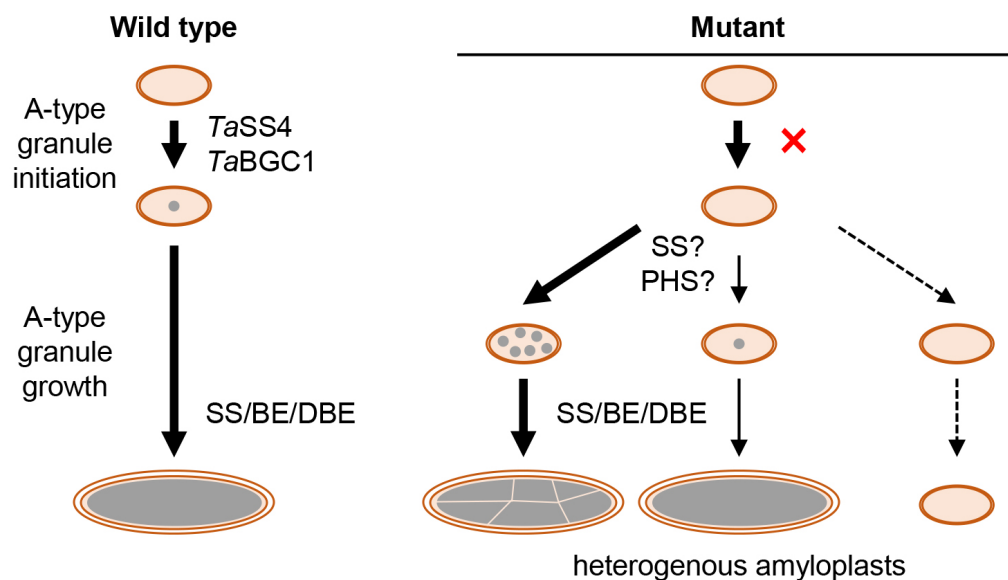


Fig. 11. Model of *TaSS4* action in endosperm starch initiation. *TaSS4* and *TaBGC1* are required for the control of normal A-type granule initiation. We propose that they establish a single granule initial that serves as the preferred substrate of other biosynthesis enzymes for building an A-type granule. In the absence of the granule initial, the other biosynthesis enzymes begin to elongate other available substrates such as soluble maltooligosaccharides, which results in the initiation of an undefined number of granules. This leads to heterogeneity among amyloplasts, where most have multiple initiations (leading to a compound granule) and some have normal A-type granules. It is possible that some amyloplasts do not initiate any starch granule, but the prevalence of this is unknown. Abbreviations are SS – starch synthase, PHS – starch phosphorylase, BE – branching enzyme, DBE – debranching enzyme.